Radboud Universiteit

GRAPHENE FLAGSHIP

Electronic structure and properties of a few-layer black phosphorus

Mikhail Katsnelson

Main collaborators:

Sasha Rudenko

Shengjun Yuan

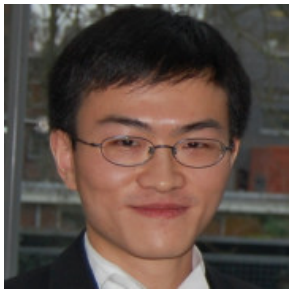

Rafa Roldan

Sergey Brener

Clément Dutreix

Zhenya Stepanov

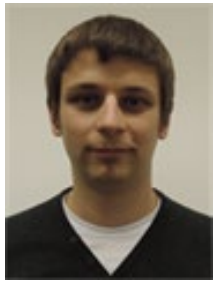

Edo van Veen

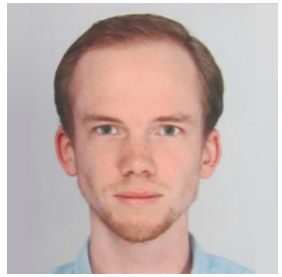

Zoo of 2D materials

Plenty of 2D materials starting from graphene

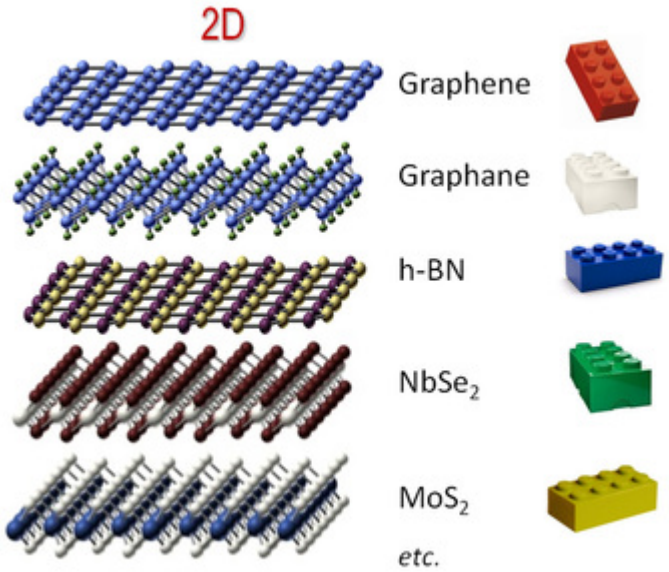

Semimetals (graphene), semiconductors, metals, superconductors, broad-gap insulators...

Graphene

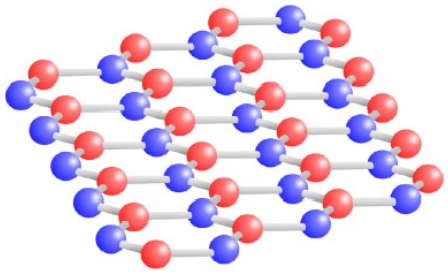

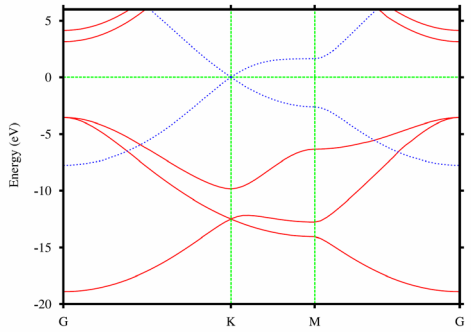

FIG. 2: (color online) Band structure of a single graphene layer. Solid red lines are σ bands and dotted blue lines are π bands.

Silicene, germanene

Buckling

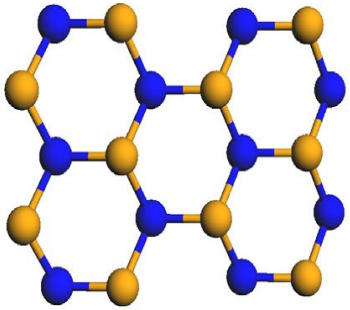

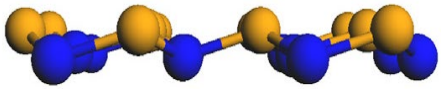

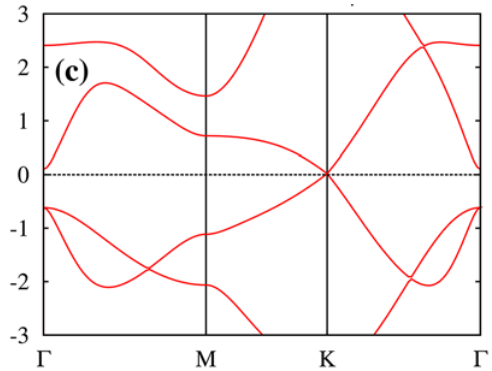

OPEN ACCESS
IOP Publishing
Journal of Physics: Condensed Matter

J. Phys.: Condens. Matter **27** (2015) 443002 (11pp)
doi:10.1088/0953-8984/27/44/443002

Topical Review

Germanene: the germanium analogue of graphene

A Acun[1,6], L Zhang[1,6], P Bampoulis[1], M Farmanbar[2], A van Houselt[1], A N Rudenko[3], M Lingenfelder[4,5], G Brocks[2], B Poelsema[1], M I Katsnelson[3] and H J W Zandvliet[1]

Zoo of 2D materials II

Antimony

PHYSICAL REVIEW B **95**, 081407(R) (2017)

Electronic properties of single-layer antimony: Tight-binding model, spin-orbit coupling, and the strength of effective Coulomb interactions

A. N. Rudenko,[1,*] M. I. Katsnelson,[1] and R. Roldán[2]

The same buckled structure as for silicene or germanene

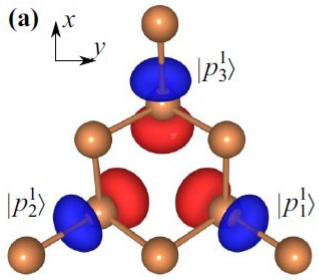

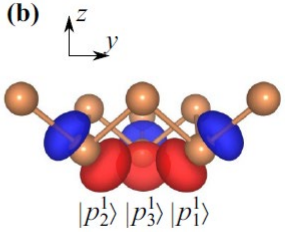

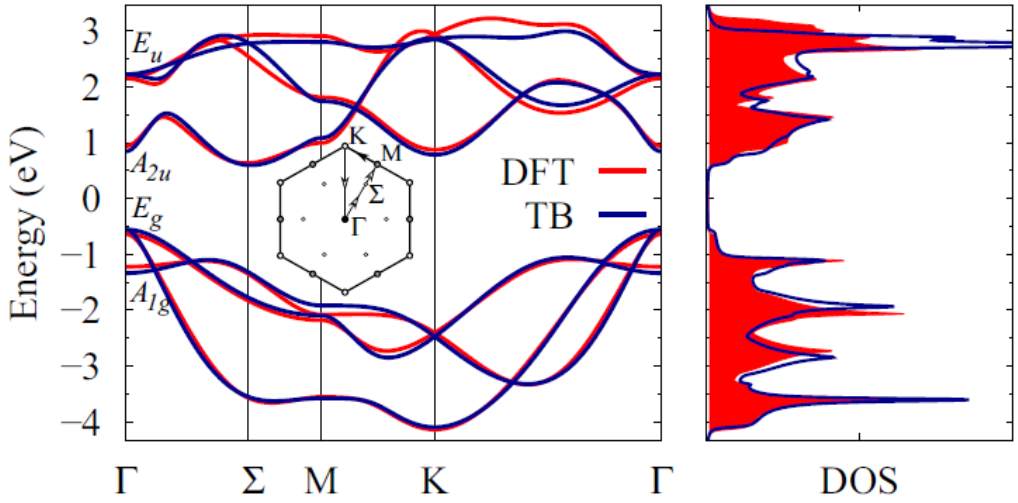

Method	$E_g^{\Gamma\Sigma}$	$E_g^{\Gamma\Gamma}$	Holes		Electrons			
			m_Γ^1	m_Γ^2	m_Γ	m_Σ^x	m_Σ^y	m_K
DFT	1.26	1.57	0.08	0.45	0.09	0.14	0.45	0.39
TB	1.15	1.40	0.06	0.44	0.06	0.13	0.42	0.36
DFT+SO	0.99	1.25	0.10	0.19	0.08	0.14	0.46	0.40
TB+SO	0.92	1.14	0.09	0.11	0.06	0.13	0.43	0.37

Semiconductor. Strong spin-orbit coupling

$$\lambda = 0.34 \text{ eV}$$

What is BP?

For historical and basic review: Ling et al, PNAS 112, 4523 (2015)

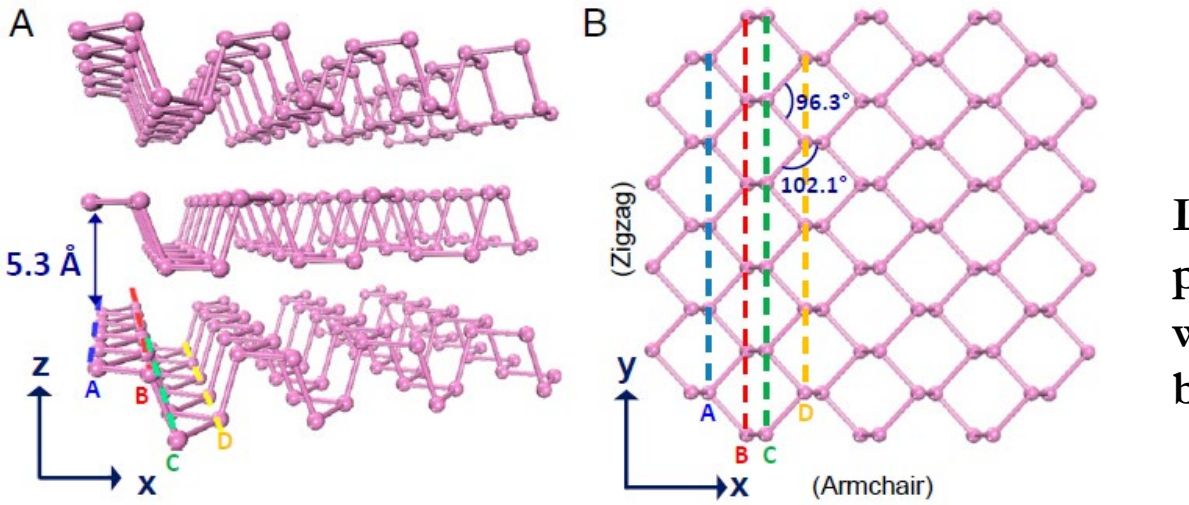

Bridgman (1914)

Black P – stable allotrope of P at ambient conditions

Layered compound, 4 atoms per unit cell, bond lengths within layer 0.222 and 0.224 nm, between layers 0.53 nm

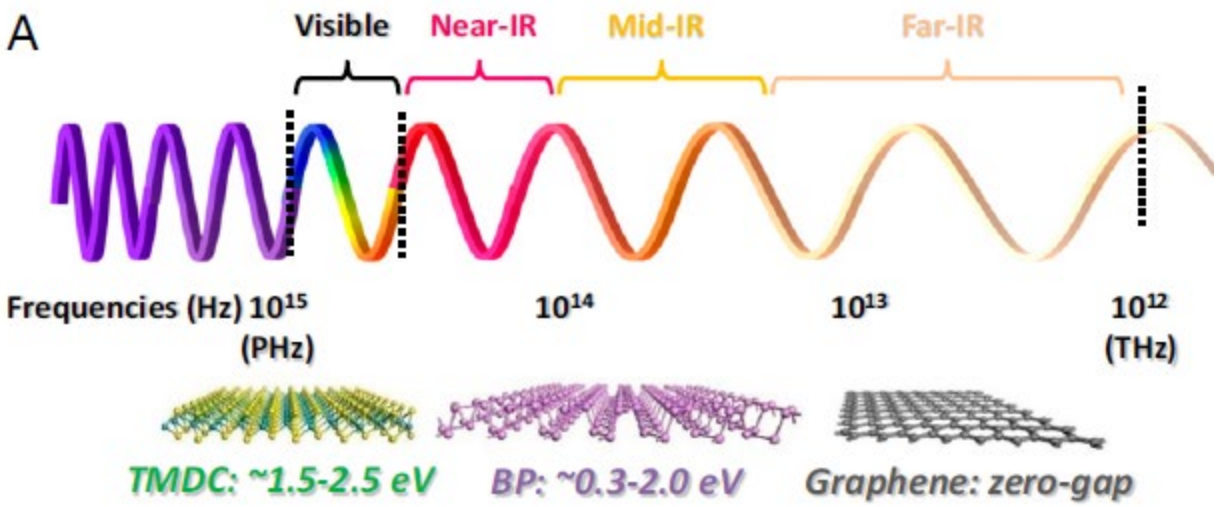

Tunable gap, depending on number of layers

Other allopropes of phosphorus

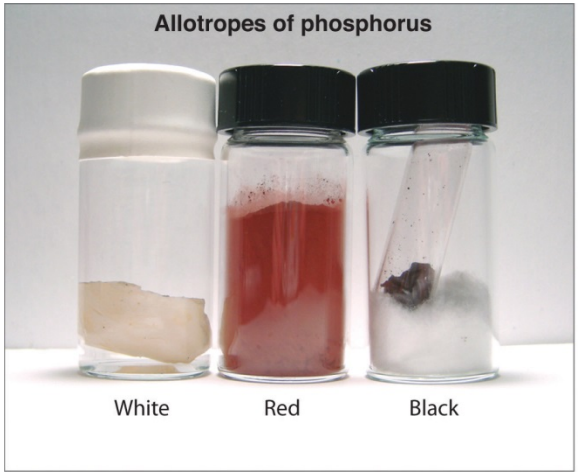

White phosphorus

Volatile waxy white solid. Dangerously reactive in air: glows with a white light and spontaneously bursts into flame.

Melting point: 44.2°C

Red phosphorus

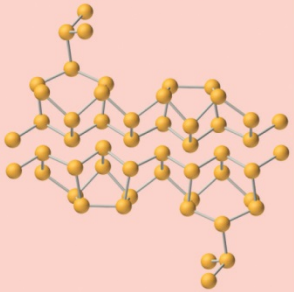

Red powder. Nonreactive with air at 25°C.

Melting point: 590°C

Black phosphorus

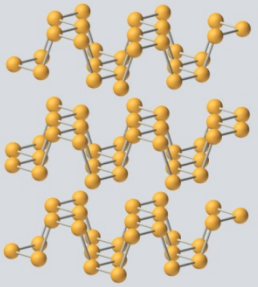

Black crystalline solid. Nonreactive with air at 25°C.

Melting point: 610°C

White phosphorus is most know to a general public (e.g., "phosphorescence")

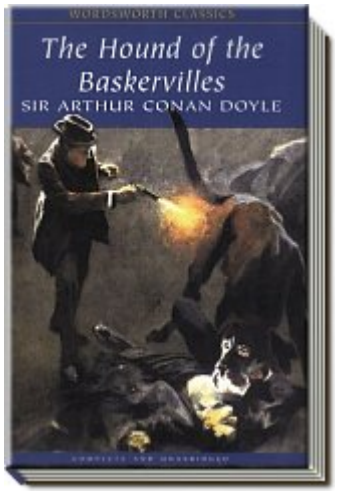

Computations of electronic structure

RAPID COMMUNICATIONS

PHYSICAL REVIEW B **89**, 201408(R) (2014)

Quasiparticle band structure and tight-binding model for single- and bilayer black phosphorus

A. N. Rudenko* and M. I. Katsnelson

PHYSICAL REVIEW B **92**, 085419 (2015)

Toward a realistic description of multilayer black phosphorus: From *GW* approximation to large-scale tight-binding simulations

A. N. Rudenko,* Shengjun Yuan, and M. I. Katsnelson

Gap problem: conventional density functional (LDA or GGA) usually strongly underestimates gaps in semiconductors – more advanced methods should be used like **GW**

Quasiparticle equation:

$$(T + V_{\mathrm{n-e}} + V_{\mathrm{H}}) + \int \underbrace{\Sigma(\mathbf{r}, \mathbf{r}', E_{nk})}_{\text{Self-energy}} \psi_{nk}(\mathbf{r}')\mathrm{d}\mathbf{r}' = \underbrace{E_{nk}}_{\text{QP energy}} \psi_{nk}(\mathbf{r})$$

Self-energy in the *GW* approximation:

$$\Sigma^{GW}(\mathbf{r}, \mathbf{r}'; \omega) = \frac{i\hbar}{2\pi} \int_{-\infty}^{\infty} \underbrace{G(\mathbf{r}, \mathbf{r}'; \omega + \omega')}_{\text{Green's function}} \underbrace{W(\mathbf{r}, \mathbf{r}'; \omega')}_{\text{Screened Coul. int.}} e^{i\omega'\eta}\mathrm{d}\omega'$$

Computations of electronic structure II

Bulk BP

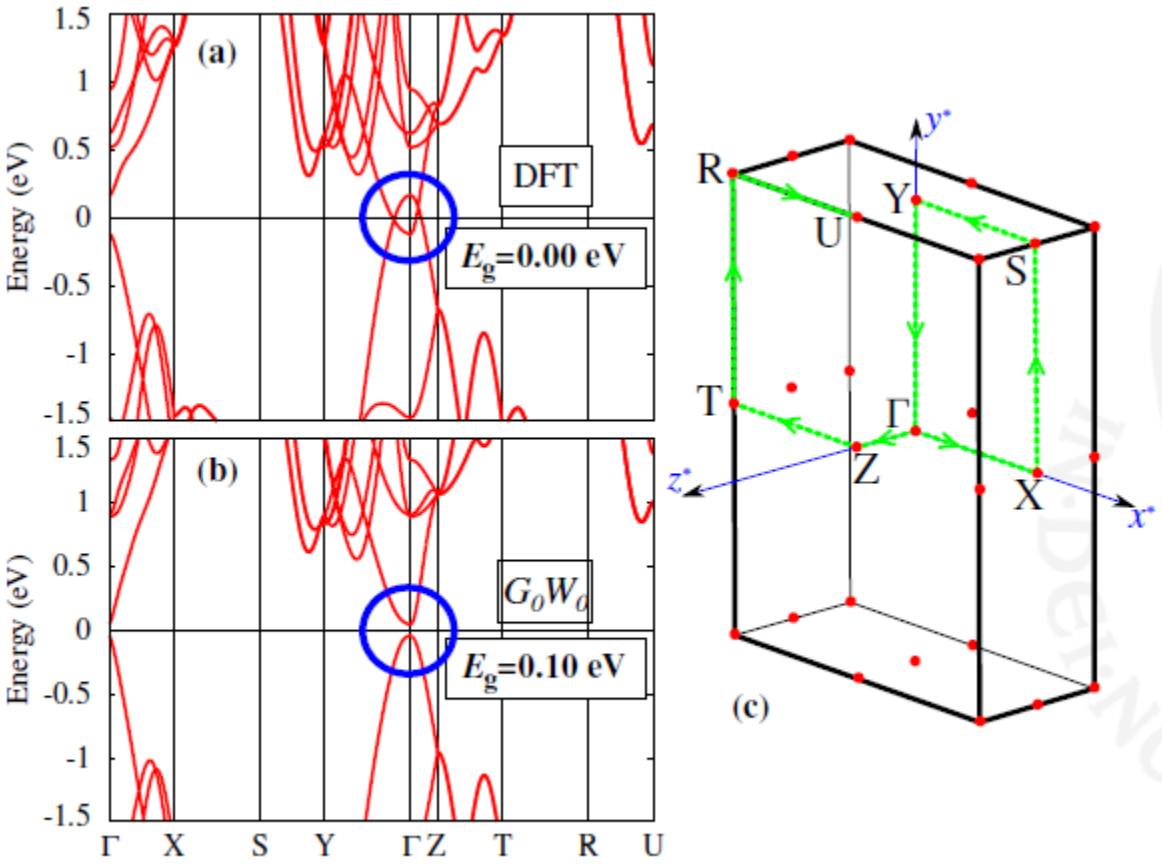

GW fixes the band gap problem

And self-consistency makes the gap accurate, 0.35 eV!

Computations of electronic structure III

TABLE I. Band gaps (in eV) for monolayer ($n = 1$), multilayer ($n = 2,3$), and bulk BP ($n = \infty$) calculated at different levels of theory. In the notation of different methods, G_0 and W_0 imply that the Green's function and screened Coulomb repulsion in the GW approach are calculated non-self-consistently on the basis of wave functions derived from density functional (GGA) or hybrid functional (HSE) calculations, whereas G means a self-consistent calculation of the Green's function. W_0' and W_0 denote that the screened Coulomb interaction is calculated by using the general plasmon pole model [39] and RPA [40], respectively.

	GW_0@GGA[a]	TB Model[a]	GW_0@GGA[b]	GW_0@HSE[c]	G_0W_0@GGA[d]	G_0W_0'@GGA[e]	HSE[f]	GGA[g]	Expt.
$n = 1$	1.85	1.84	1.94	2.41	1.60	2.00	1.00–1.91	0.80–0.91	2.05[h]
$n = 2$	1.16	1.15	~1.65	1.66	1.01	~1.30	1.01–1.23	0.45–0.60	—
$n = 3$	0.84	0.85	~1.35	1.20	0.68	~1.05	0.73–0.98	0.20–0.40	—
$n = \infty$	0.35	0.40	0.43	0.58	0.10	0.30	0.18–0.39	0.00–0.15	0.31–0.35[i]

[a]This work.

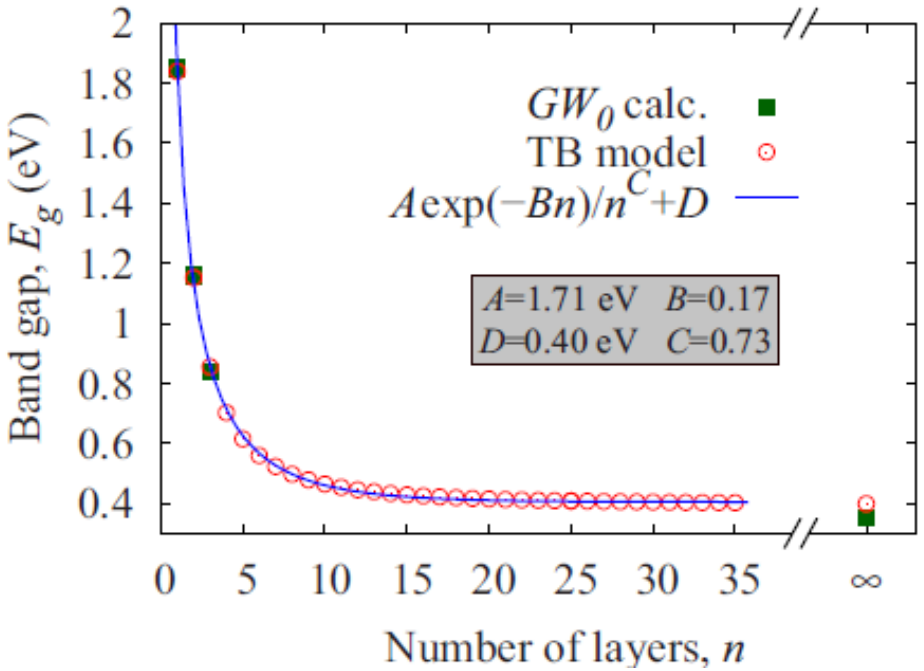

A very strong dependence of the gap on number of layers!

Computations of electronic structure IV

Cohesive energy: QMC calculations

DOI: 10.1021/acs.nanolett.5b03615
Nano Lett. 2015, 15, 8170–8175

The Nature of the Interlayer Interaction in Bulk and Few-Layer Phosphorus

L. Shulenburger,[†] A.D. Baczewski,[†] Z. Zhu,[‡] J. Guan,[‡] and D. Tománek*[,‡]

VdW interactions: weak and can hardly be described by conventional density functional

How can it be? How weak cohesive energy is consistent with a huge dependence of interlayer hopping to the gap?!

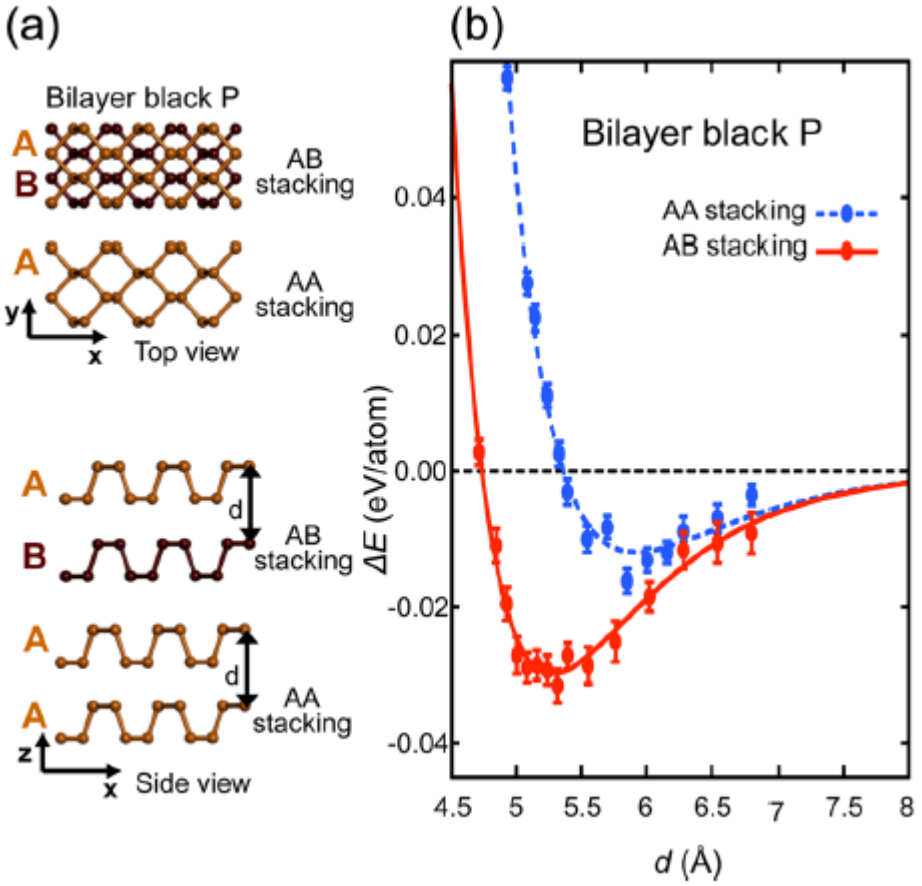

Computations of electronic structure V

GW is qualitatively important also for single layer

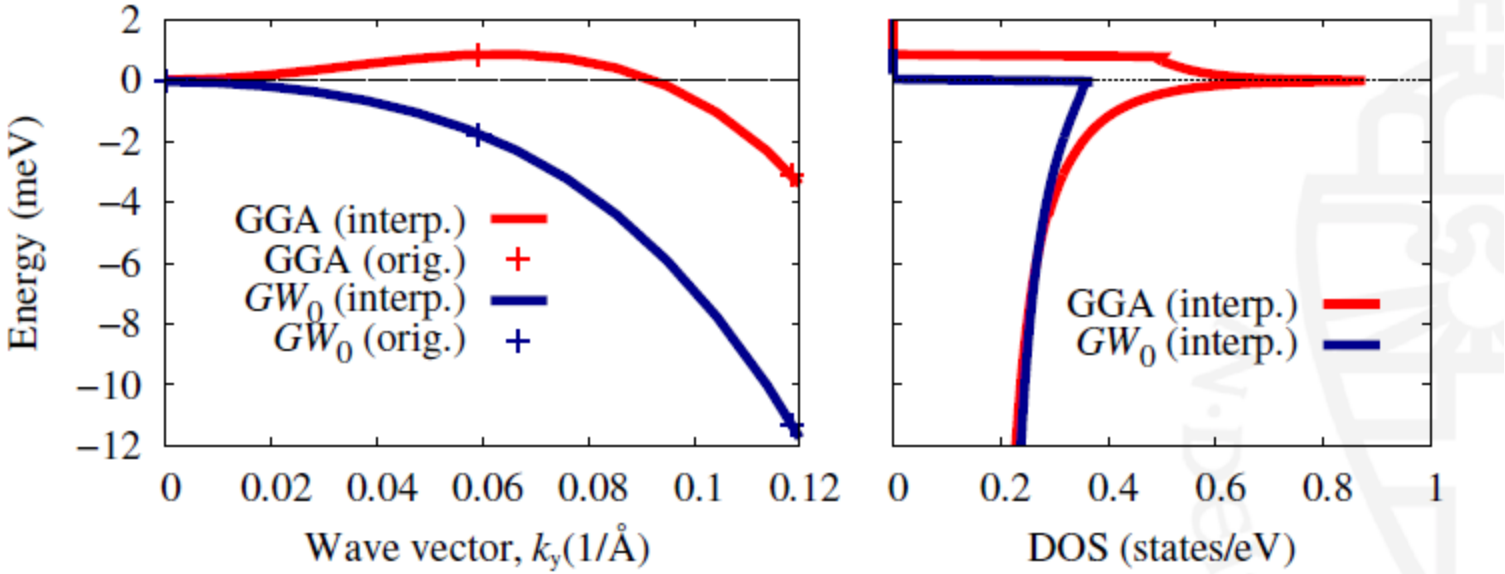

GW predicts a *direct* band gap

Mapping on tight binding model I

Single layer BP

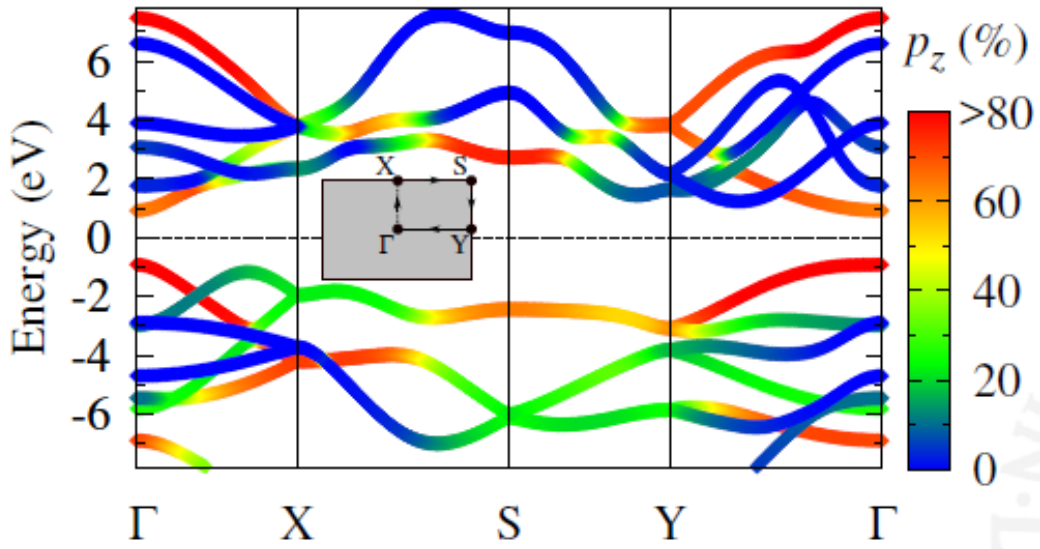

- Valence and conduction band edges are isolated
- ...and have predominantly p_z character

$H^{\mathbf{k}}_{GW}$ *multiorbital Hamiltonian* → $H^{\mathbf{R}}_{TB}$ *single-orbital Hamiltonian*

Mapping on tight binding model II

Minimal model for single-layer BP (phosphorene)

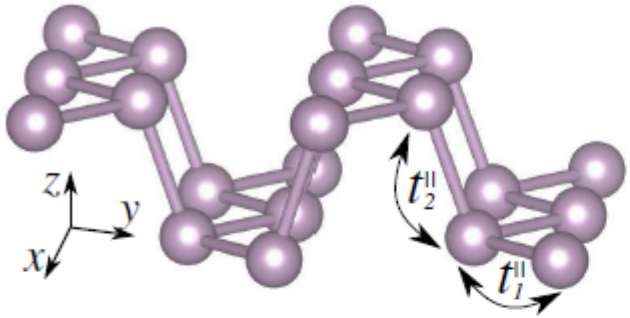

$$t_1^{||} \approx -1.5 \text{ eV} \; ; \; t_2^{||} \approx +3.7 \text{ eV}$$

$$H = \sum_{i \neq j} t_{ij}^{||} c_i^\dagger c_j$$

$$\underbrace{\Delta_g^{(1)}(\Gamma)}_{\text{Band gap}} \approx 2t_2^{||} + 4t_1^{||}$$

Band gap appearance criterion: $t_2^{||} > 2|t_1^{||}|$

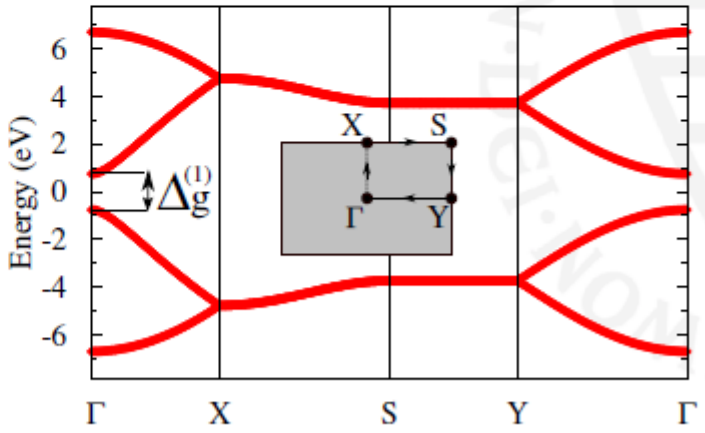

A. Rudenko, M. Katsnelson, PRB **89**, 201408 (2014)

Mapping on tight binding model III

Minimal model for bilayer BP

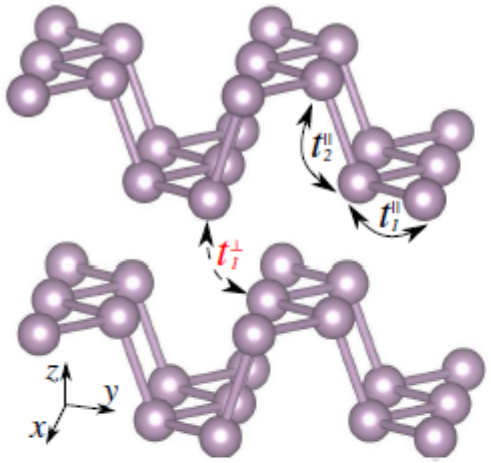

$$H = \underbrace{\sum_{i \neq j} t_{ij}^{\parallel} c_i^{\dagger} c_j}_{\text{intralayer term}} + \underbrace{\sum_{i \neq j} t_{ij}^{\perp} c_i^{\dagger} c_j}_{\text{interlayer term}}$$

$$t_1^{\parallel} \approx -1.5\text{eV} \; ; \; t_2^{\parallel} \approx +3.7\text{eV} \; ; \; t_1^{\perp} \approx 0.5\text{eV}$$

$t_1^{\perp}$ accounts for the narrowing of a gap in multilayer BP

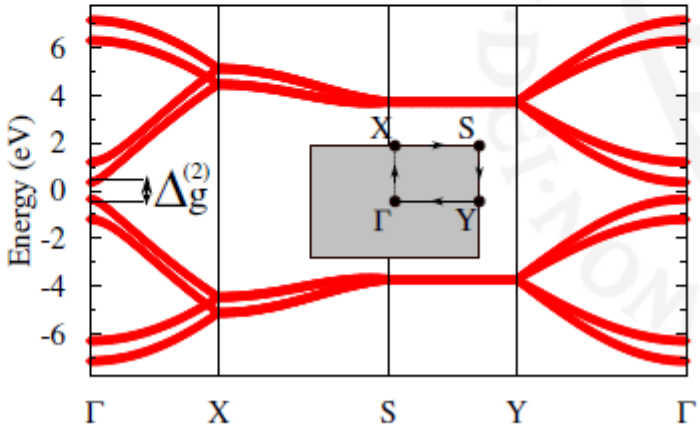

A. Rudenko, M. Katsnelson, PRB **89**, 201408 (2014)

Mapping on tight binding model IV

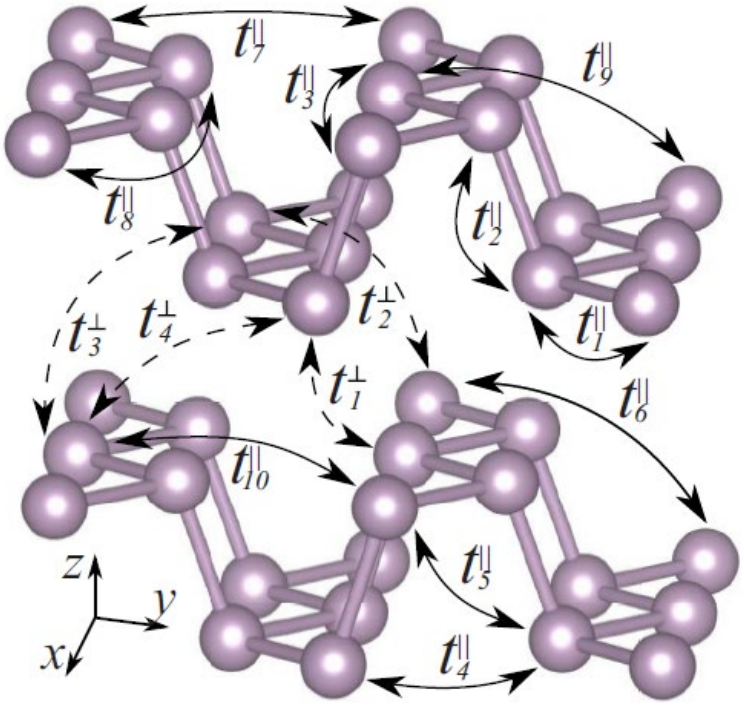

TABLE II. Intralayer ($t^{\parallel}$) and interlayer ($t^{\perp}$) hopping parameters (in eV) obtained in terms of the TB Hamiltonian [Eq. (1)] for multilayer BP. d and N_c denote the distances between the corresponding interacting lattice sites and coordination numbers for the given distance, respectively. The hoppings are schematically shown

	Intralayer				Intralayer				Interlayer		
No.	$t^{\parallel}$ (eV)	d (Å)	N_c	No.	$t^{\parallel}$ (eV)	d (Å)	N_c	No.	$t^{\perp}$ (eV)	d (Å)	N_c
1	−1.486	2.22	2	6	0.186	4.23	1	1	0.524	3.60	2
2	3.729	2.24	1	7	−0.063	4.37	2	2	0.180	3.81	2
3	−0.252	3.31	2	8	0.101	5.18	2	3	−0.123	5.05	4
4	−0.071	3.34	2	9	−0.042	5.37	2	4	−0.168	5.08	2
5	−0.019	3.47	4	10	0.073	5.49	4	5	0.000	5.44	1

The main difference with graphene: a very large and positive second-neighbour hopping in plane; interlayer hopping is roughly of the same order of magnitude

Effect of interlayer bias: anisotropic Dirac cones

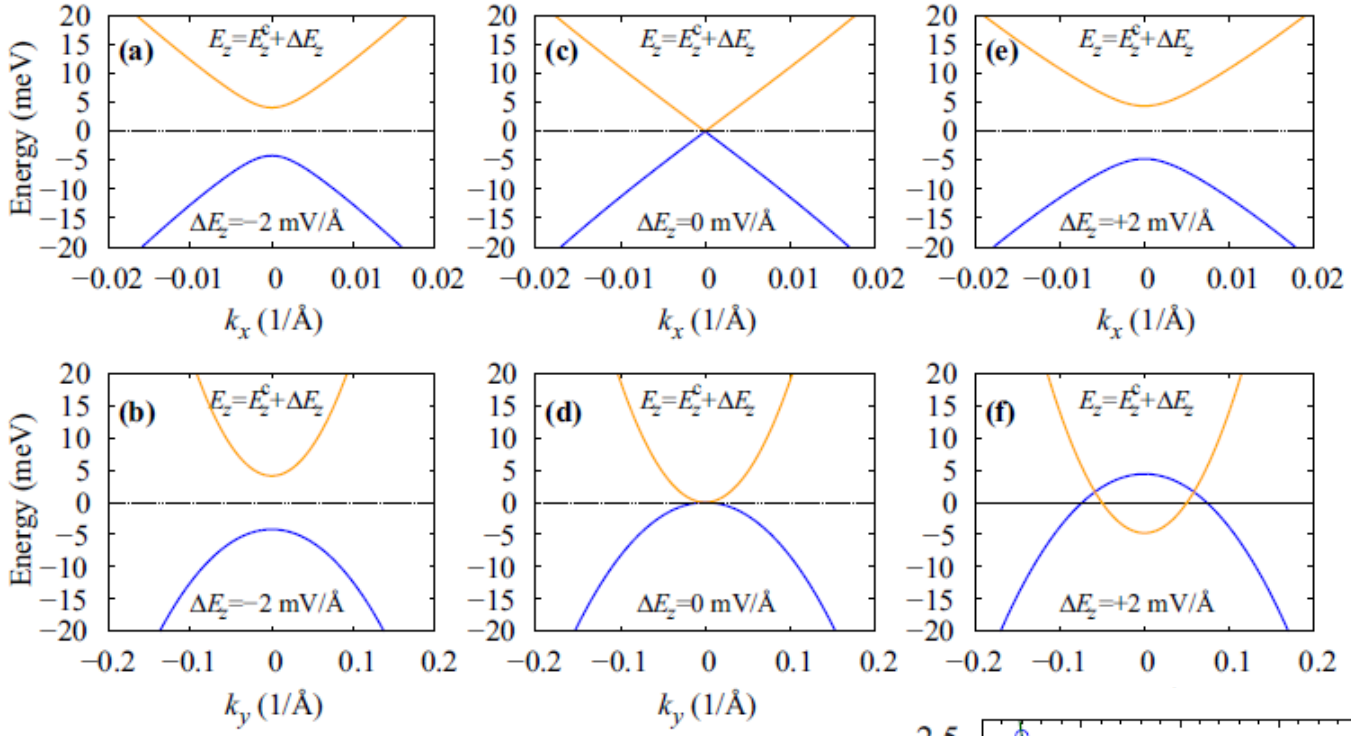

Linear crossing in *x* direction and parabolic in *y* direction

Bias leads to gap opening and formation of anisotropic conical points

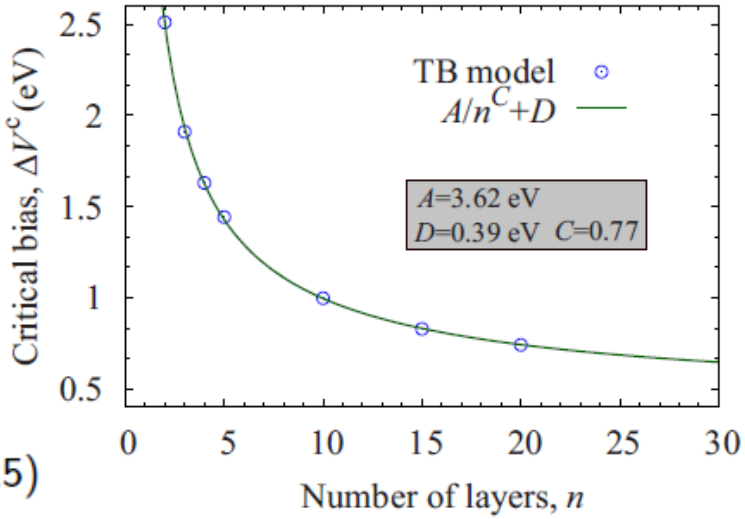

A. Rudenko, S. Yuan, M. Katsnelson, PRB **92**, 085419 (2015)

Effect of interlayer bias: anisotropic Dirac cones II

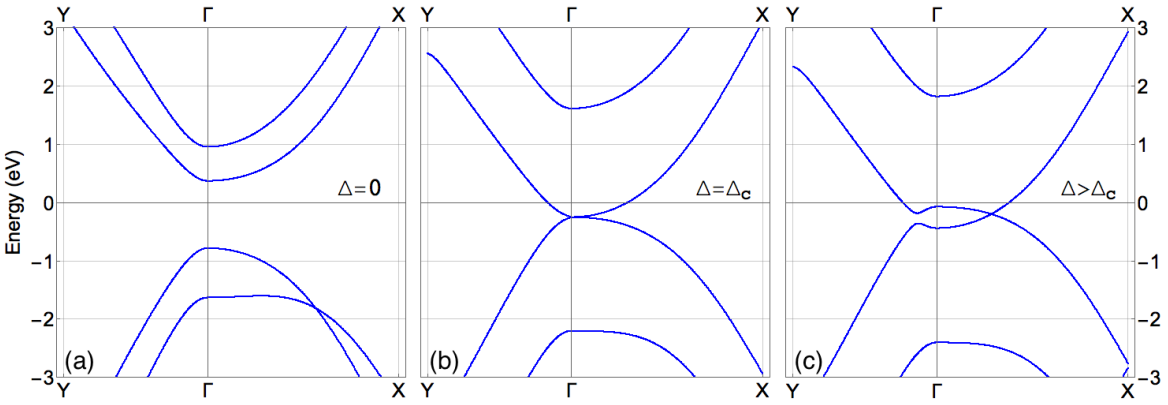

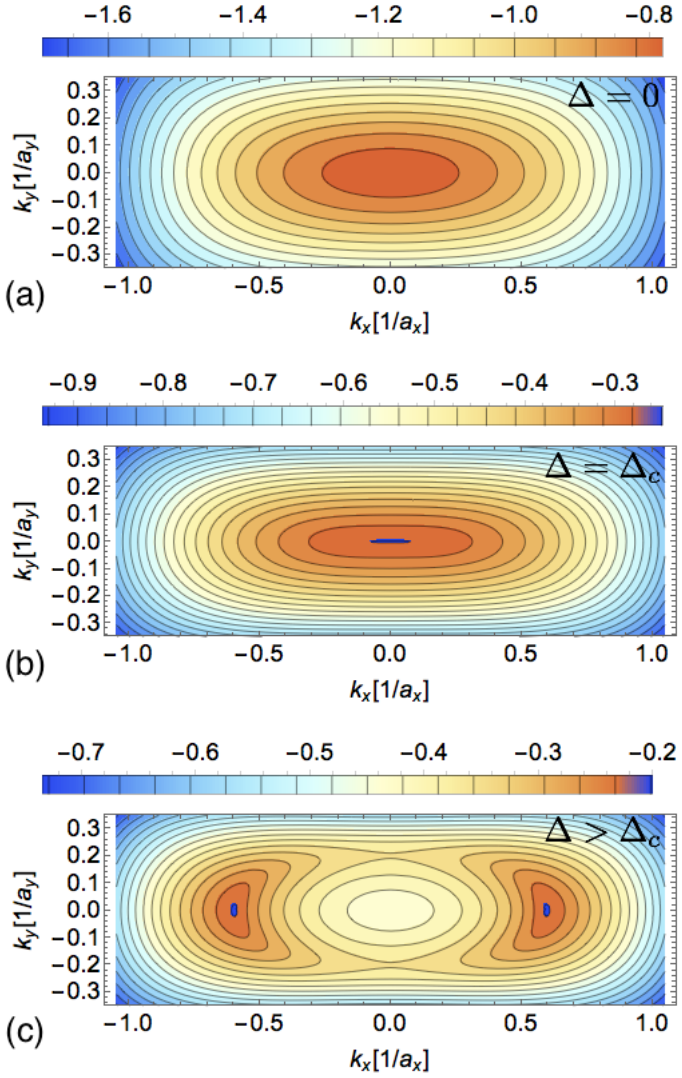

Insulator-semimetal transition with formation of anisotropic Dirac cones

S. Yuan, MIK, R. Roldan, PRB 93, 245433 (2016)

Experiment: K deposite

Observation of tunable band gap and anisotropic Dirac semimetal state in black phosphorus

Jimin Kim,[1] Seung Su Baik,[2,3] Sae Hee Ryu,[1,4] Yeongsup Sohn,[1,4] Soohyung Park,[2]
Byeong-Gyu Park,[5] Jonathan Denlinger,[6] Yeonjin Yi,[2]
Hyoung Joon Choi,[2,3] Keun Su Kim[1,4]*

SCIENCE

14 AUGUST 2015 • VOL 349 ISSUE 6249 723

ARPES

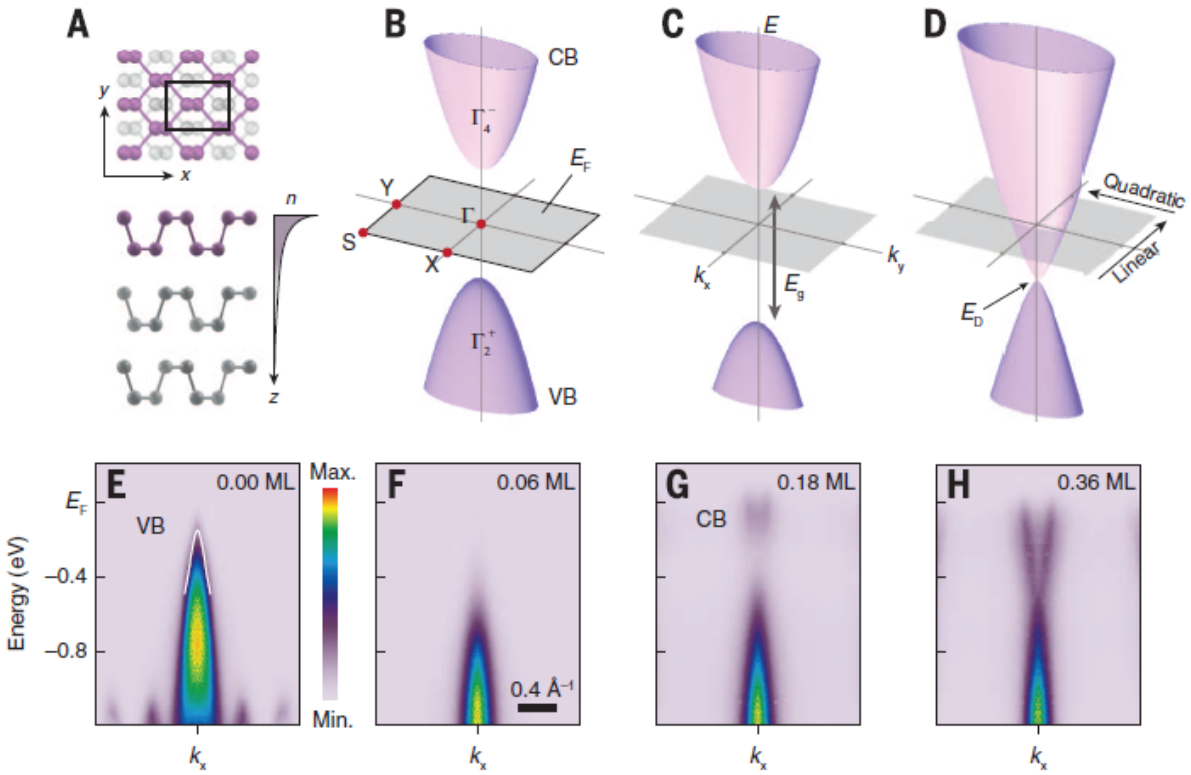

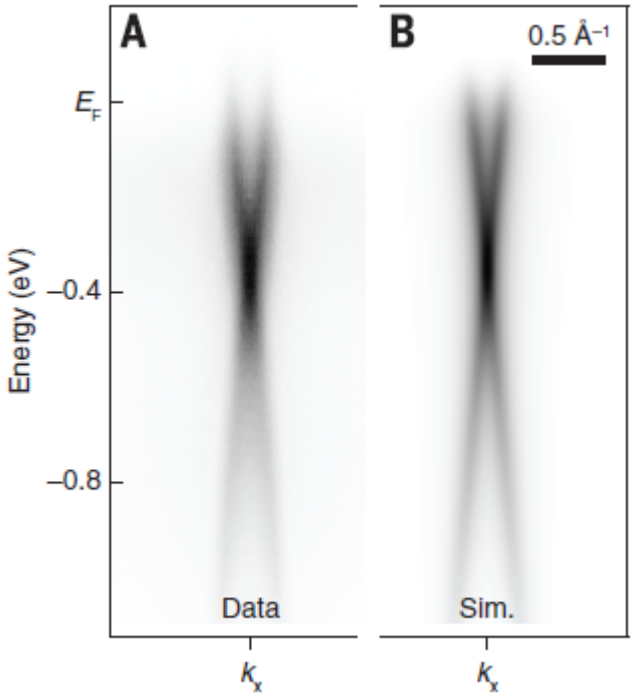

High-frequency laser fields

Quickly oscillating strong electric field means quickly oscillating effective hopping

$$t_{ij} \to t_{ij} \exp\left\{ \frac{ie}{\hbar c} \int_{\vec{R}_j}^{\vec{R}_i} d\vec{r}\,' \vec{A}(\vec{r}\,', t) \right\}$$

At very high frequency effective *static* Hamiltonian should exist

Classical analog: Kapitza pendulum

One needs to develop efficient perturbative theory in inverse frequency of the laser field

In classical mechanics: Bogoliubov, Krylov ...

Development for matrix Hamiltonians: A. P. Itin & A. I. Neishtadt, Phys. Lett. A 378, 822 (2014)

http://butikov.faculty.ifmo.ru/Russian/ParamPendulumKIO.pdf

Laser-induced topological transitions

C. Dutreix, E. A. Stepanov & MIK, Phys. Rev. B 93, 241404(R) (2016)

In bilayer, electric bias creates insulator-semimetal transition; but with high-frequency laser field one can make it for the single layer

Averaging over high-frequency field:

A. P. Itin & MIK, Phys. Rev. Lett. 115, 075301 (2015)

C. Dutreix & MIK, Phys. Rev. B 95, 024306 (2017)

High-frequency expansion (in $1/\Omega$) for the effective *static* Hamiltonian

$$\tilde{H}_1 = H_0, \quad \tilde{H}_2 = -\frac{1}{2}\sum_{m\neq 0}\frac{[H_m, H_{-m}]}{m},$$

$$\tilde{H}_3 = \frac{1}{2}\sum_{m\neq 0}\frac{[[H_m, H_0], H_{-m}]}{m^2} + \frac{1}{3}\sum_{m\neq 0}\sum_{n\neq 0,m}\frac{[[H_m, H_{n-m}], H_{-n}]}{mn},$$

$$H_m = \int_{-\pi}^{+\pi}\frac{d\tau}{2\pi}e^{im\tau}H(\tau)$$

Very important: NN and NNN hopping are renormalized differently, and both are very relevant fpr the electronic structure!

Laser-induced topological transitions II

Single-particle Hamiltonian (only bands), Peierls substitution

$$\mathbf{A}(t) = (A_x \cos \Omega t, A_y \sin[\Omega t - \phi], 0)$$

Second-order effective static Hamiltonian

On can pass from band insulator to topological insulator or to semimetal

Elliptic polarization: topological insulator
Linear polarization: semimetal, no gap

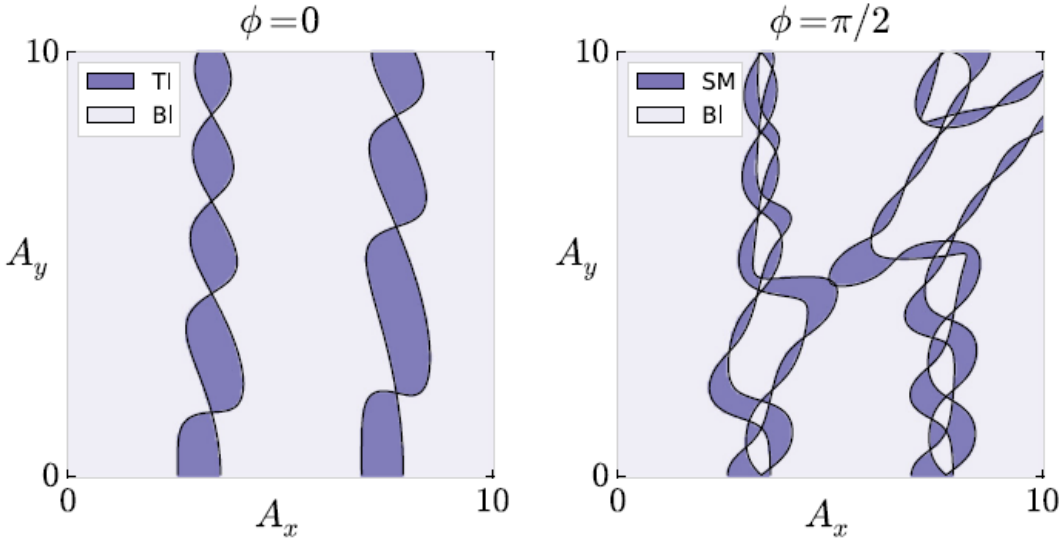

FIG. 3. Phase diagrams for electric fields with elliptic (left) and linear (right) polarizations. Light purple areas refer to band insulating (BI) phases characterized by $e^{i\gamma_C} = +1$. Dark purple areas correspond to semimetallic (SM) and topological insulating (TI) phases in which $e^{i\gamma_C} = -1$. Components A_x and A_y are given in Å^{-1}.

Lowest-energy bands in semimetallic phase

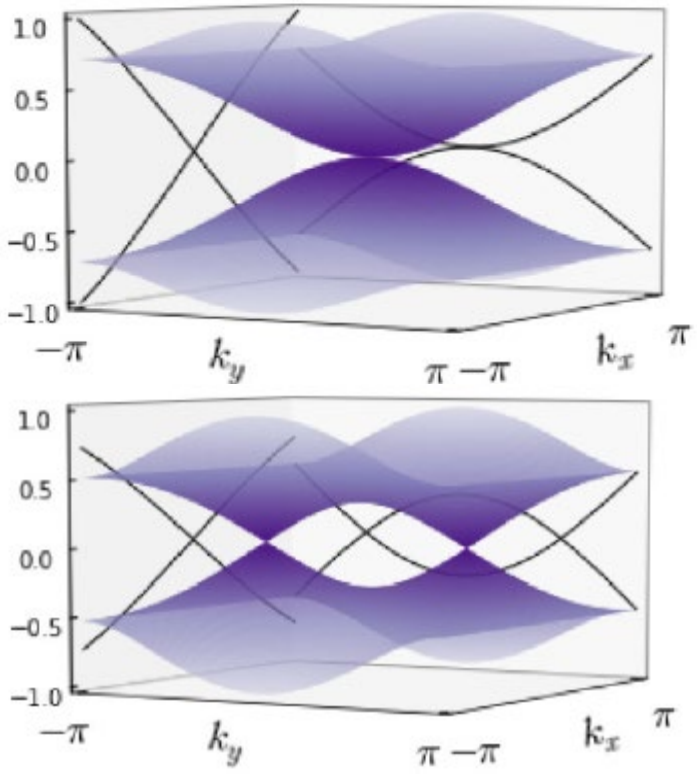

Optics

Two approaches for $\sigma_{xx}(\omega)$:

1. **k**-space (based on *GW* approximation)

$$\sigma_{\alpha\beta}(\omega) = \frac{i\hbar}{N_k \Omega} \sum_{\mathbf{k}} \sum_{mn} \frac{f_{m\mathbf{k}} - f_{n\mathbf{k}}}{\varepsilon_{m\mathbf{k}} - \varepsilon_{n\mathbf{k}}} \frac{\langle n\mathbf{k}|j_\alpha|m\mathbf{k}\rangle \langle m\mathbf{k}|j_\beta|n\mathbf{k}\rangle}{\varepsilon_{m\mathbf{k}} - \varepsilon_{n\mathbf{k}} - (\hbar\omega + i\eta)}$$

2. **R**-space (tight-binding propagation method)

$$\sigma_{\alpha\beta}(\omega) = \lim_{\epsilon \to 0^+} \frac{e^{-\tilde{\beta}\omega} - 1}{\omega\Omega} \int_0^\infty e^{-\epsilon t} \sin \omega t \times 2 \operatorname{Im} \langle \varphi | f(\mathcal{H}) J_\alpha(t) [1 - f(\mathcal{H})] J_\beta | \varphi \rangle \, \mathrm{d}t$$

Chebyshev polynom expansion, etc. – up to 10^9 sites

Successfully applied to graphene

PHYSICAL REVIEW B **82**, 115448 (2010)

Modeling electronic structure and transport properties of graphene with resonant scattering centers

Shengjun Yuan,[1,*] Hans De Raedt,[2,†] and Mikhail I. Katsnelson[1,‡]

Optics II

Two approaches for $\sigma_{xx}(\omega)$:

- *GW* (**k**-space)

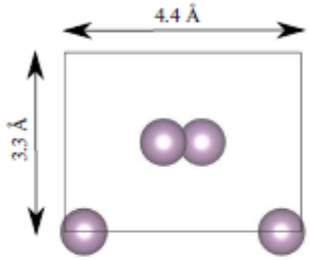

primitive cell
(four atoms)

- TB (**R**-space)

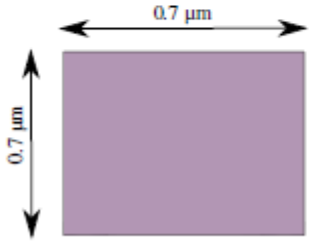

large supercell
($\sim 10^7$ atoms)

Excellent agreement up to $\omega \sim 2.5$ eV

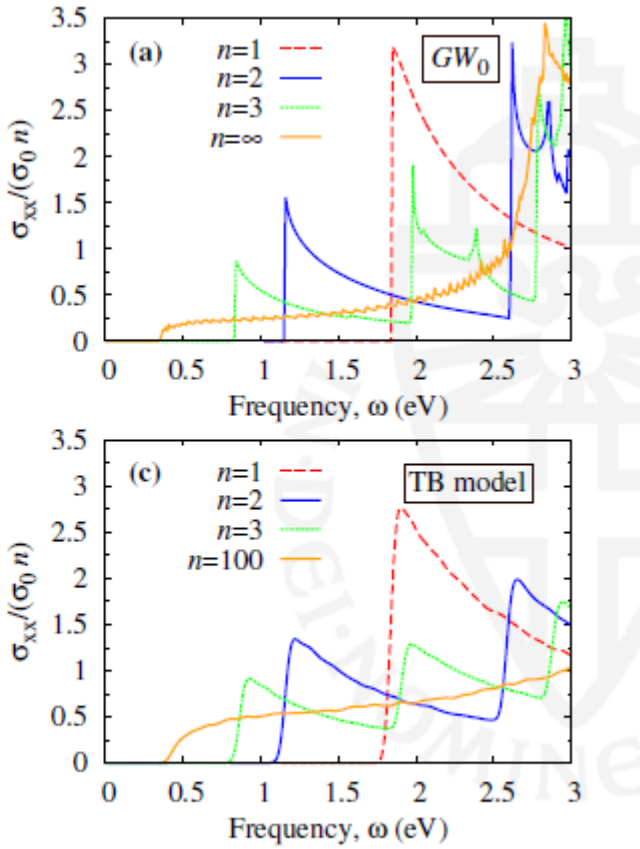

A. Rudenko, S. Yuan, M. Katsnelson, PRB **92**, 085419 (2015)

Hyperbolic plasmons

Just to remind: crystallooptics

$$\vec{k} = k_0 \vec{n}, \qquad k_0 = \frac{\omega}{c} \qquad \det\left| n^2 \delta_{ij} - n_i n_j - \varepsilon_{ij}(\omega) \right| = 0$$

$$\varepsilon_{ij}(\omega) = \delta_{ij} + \frac{4\pi i}{\omega}\sigma_{ij}(\omega)$$

Main axes $\varepsilon_{ij} = \varepsilon_i \delta_{ij}$

If $\varepsilon_x \varepsilon_y < 0$

$$n_z = 0$$
$$n^2 = \varepsilon_z$$
$$\frac{n_x^2}{\varepsilon_y} + \frac{n_y^2}{\varepsilon_x} = 1$$

$$\frac{k_x^2}{|\varepsilon_y|} = \frac{k_y^2}{|\varepsilon_x|}, \qquad k >> k_0 \qquad (c \to \infty)$$

Hyperbolic plasmons

Hyperbolic plasmons in black P

E. Van Veen, A. Nemilentsau, A. Kumar, R. Roldan, MIK, T. Low, S. Yuan, Phys. Rev. Appl. 12, 014011 (2019)

Black P is anisotropic – one can find the region where $\varepsilon_x \varepsilon_y < 0$

Manipulations by strain

$$t_{ij}(\mathbf{r}_{ij}) = t_{ij}(\mathbf{r}_{ij}^0)\left(1 - \beta_{ij}\frac{|\mathbf{r}_{ij} - \mathbf{r}_{ij}^0|}{|\mathbf{r}_{ij}^0|}\right)$$

Or by optical gain (nonequilibrium occupation)

Quasi-equilibrium distribution

$$n_F(E) = \theta(E) f(E + \frac{E_g}{2} + \Delta\mu) + \theta(-E) f(E - \frac{E_g}{2} - \Delta\mu)$$

$$f(E-\mu) = \frac{1}{e^{(E-\mu)/kT} + 1} \qquad T = 300 \text{ K}$$

Hyperbolic plasmons in black P II

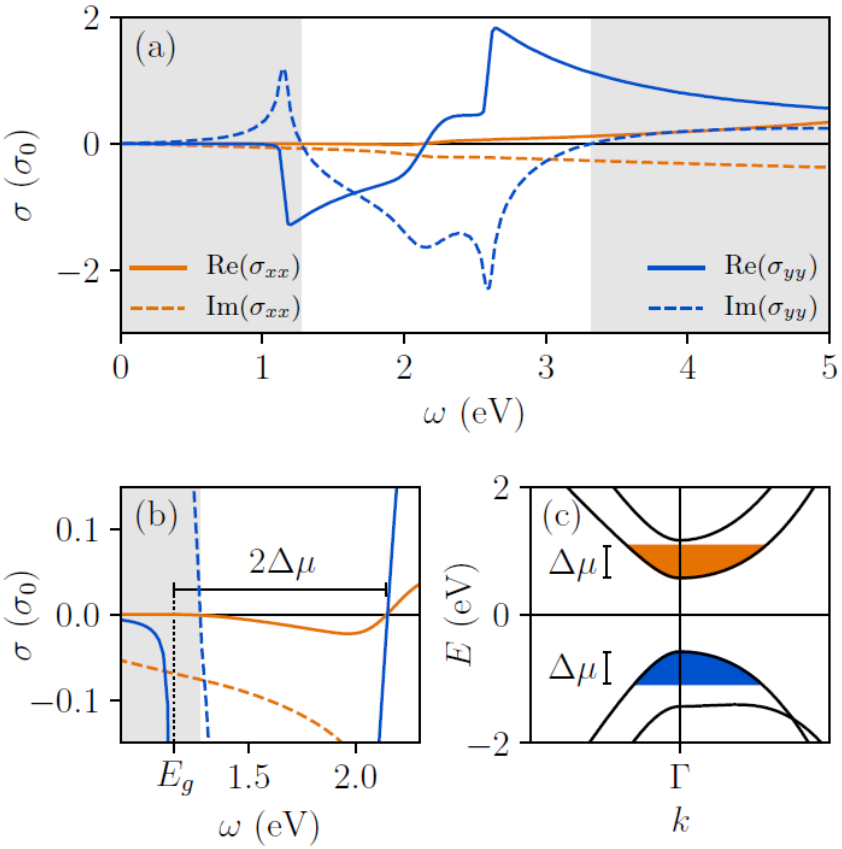

FIG. 2. (a) The optical conductivity of bilayer black phosphorus with photo-doping $\Delta\mu = 0.5$ eV. (b) A close-up of the region where $\mathrm{Re}(\sigma_{yy}) < 0$, showing a new hyperbolic region (shaded) for $\omega < 1.27$ eV. (c) The corresponding band structure around the Γ-point, with the population-inverted pockets shown in blue and orange.

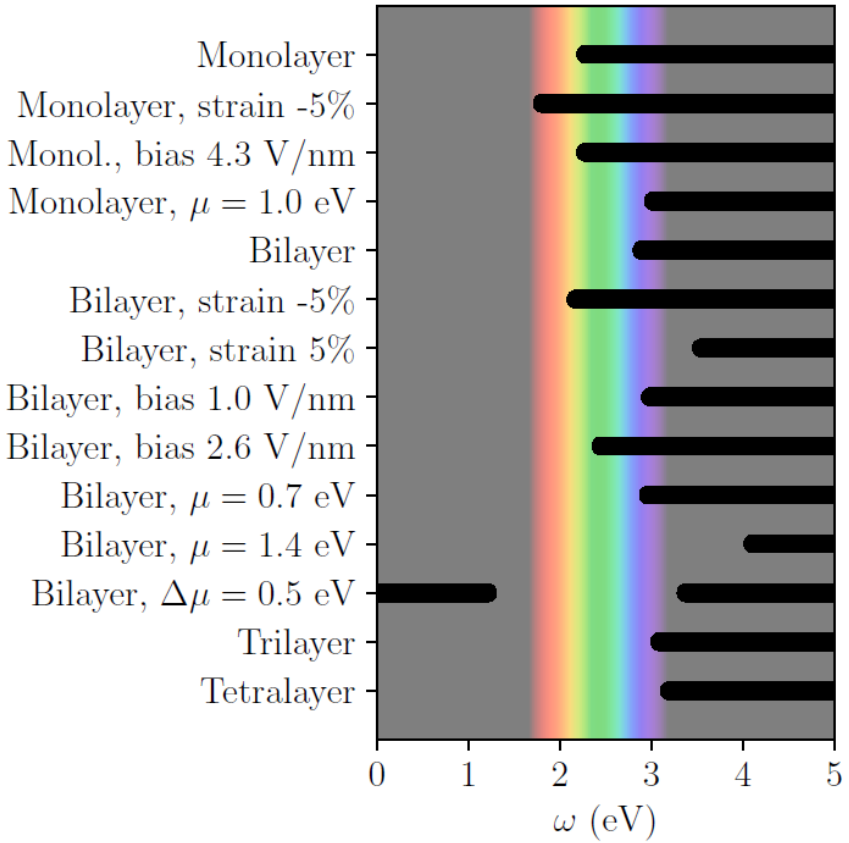

FIG. 3. The hyperbolic region (indicated in black lines) for different tuning parameters. The visual spectrum is indicated in color.

$$\sigma_0 = \frac{\pi e^2}{2h}$$

One can manipulate black (hyperbolic) regions

Large scale TB simulations for disordered BP

PHYSICAL REVIEW B **91**, 115436 (2015)

Transport and optical properties of single- and bilayer black phosphorus with defects

Shengjun Yuan,* A. N. Rudenko, and M. I. Katsnelson

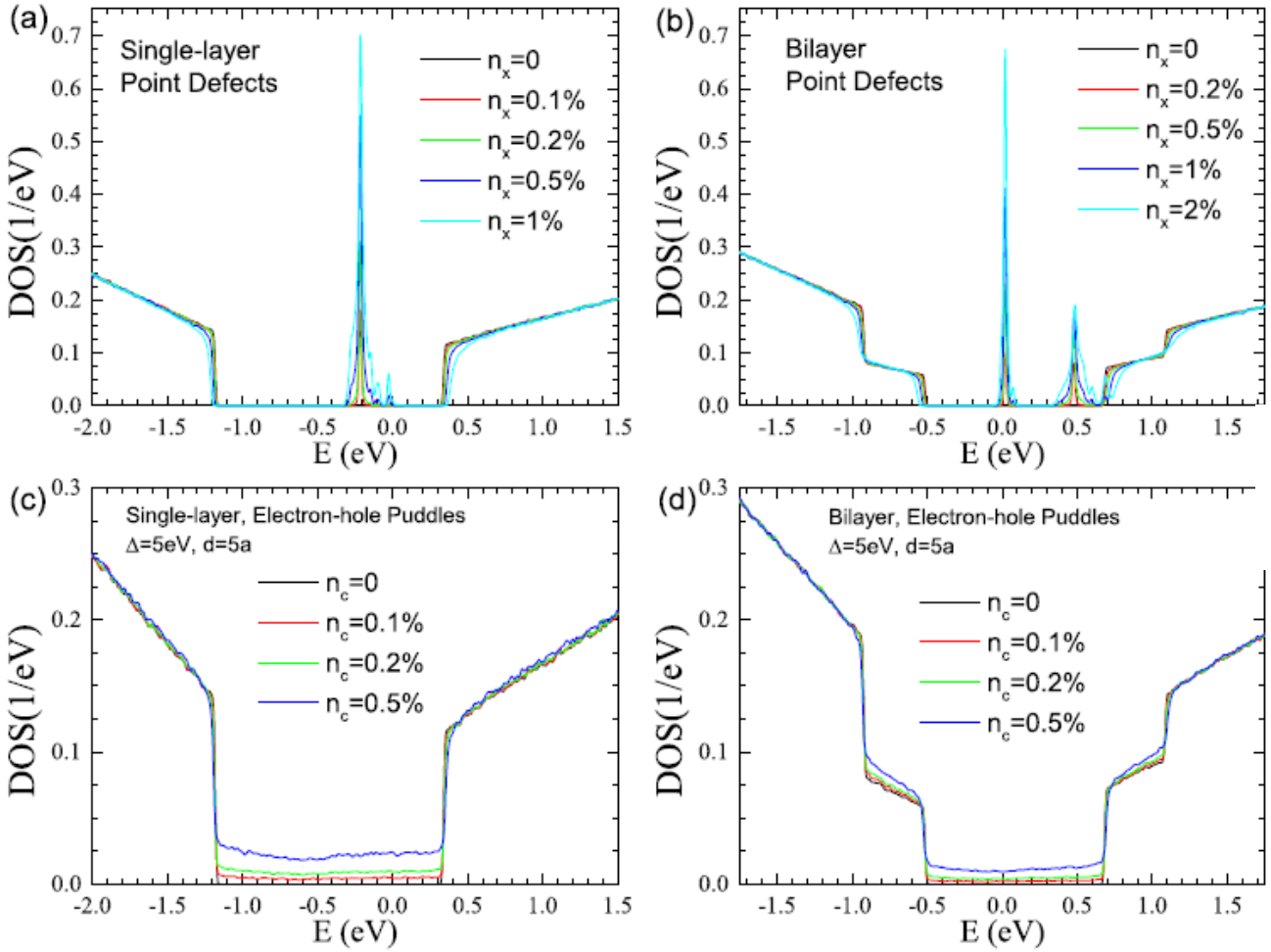

Point defects: missing atoms

Puddles: Gaussian electrostatic potential

$$v_i = \sum_{k=1}^{N_{\mathrm{imp}}^{v}} U_k \exp\left(-\frac{|\mathbf{r}_i - \mathbf{r}_k|^2}{2d^2}\right)$$

STM observation of vacancy states

Probing Single Vacancies in Black Phosphorus at the Atomic Level

Brian Kiraly, Nadine Hauptmann, Alexander N. Rudenko, Mikhail I. Katsnelson, and Alexander A. Khajetoorians*

NANO LETTERS

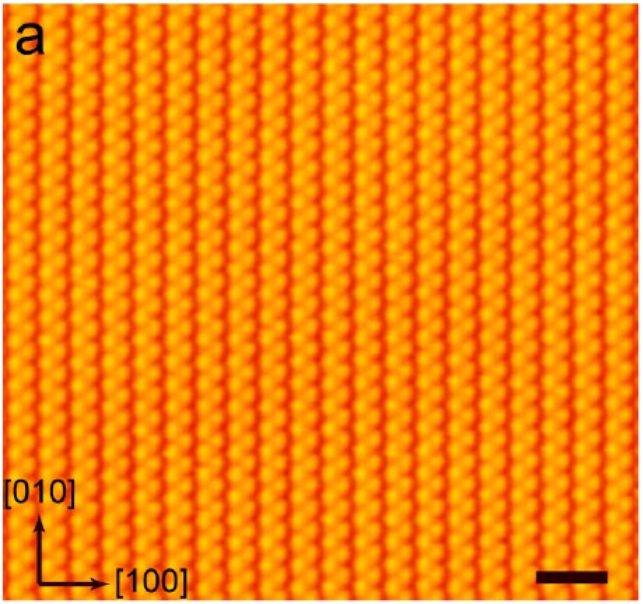

STM image of bulk black P – atomically flat surface

Figure 2. (a) Three-dimensional representation of a constant-current STM image with a distribution of single vacancies in black phosphorus (V_S = −0.1 V, I_t = 200 pA, size = 62 nm × 48 nm, color bar = 0–0.2 nm). (Inset) Line profiles taken across the vacancies labeled 1L, 2L, and 3L in (a). Constant-current STM image of a single vacancy at (b) sublattice A and (c) at sublattice B (V_S = −0.1 V, I_t = 200 pA, scale bar = 2 nm). (d) Tight-binding calculations of the charge density of a single vacancy in black phosphorus located at (d) sublattice site A and (e) sublattice site B (scale bar = 1 nm).

Comparison with calculations allows to attribute peaks to vacancies

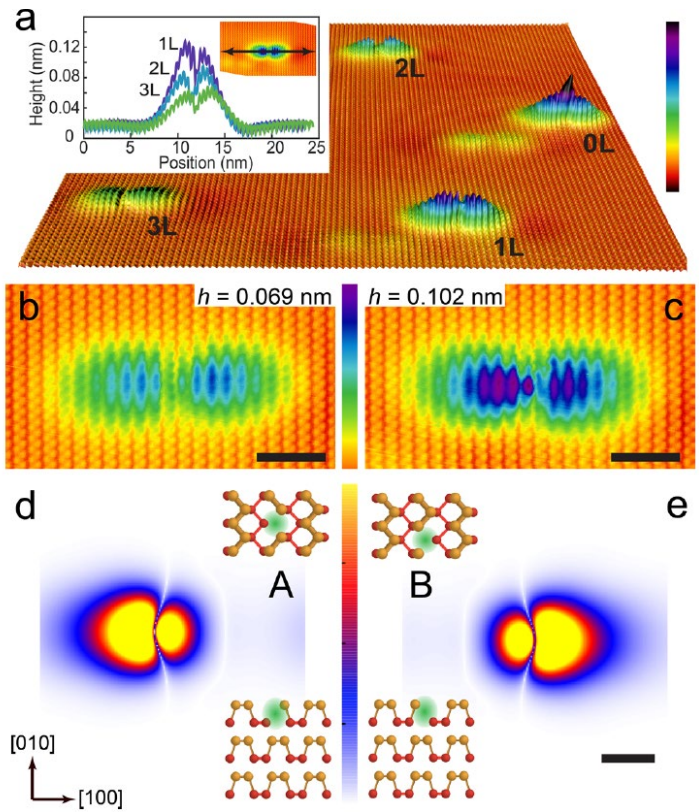

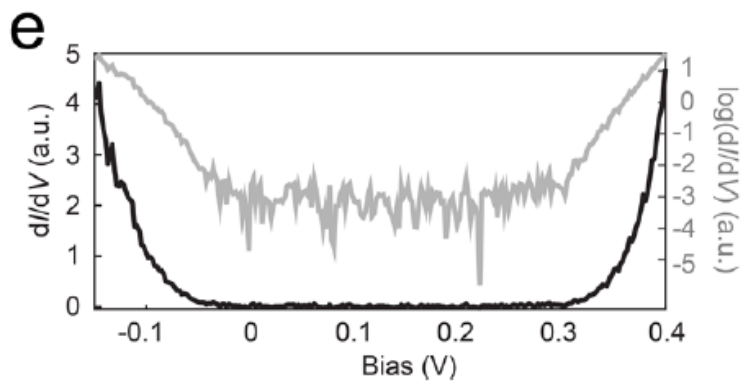

Gap 0.32 eV

STM observation of vacancy states II

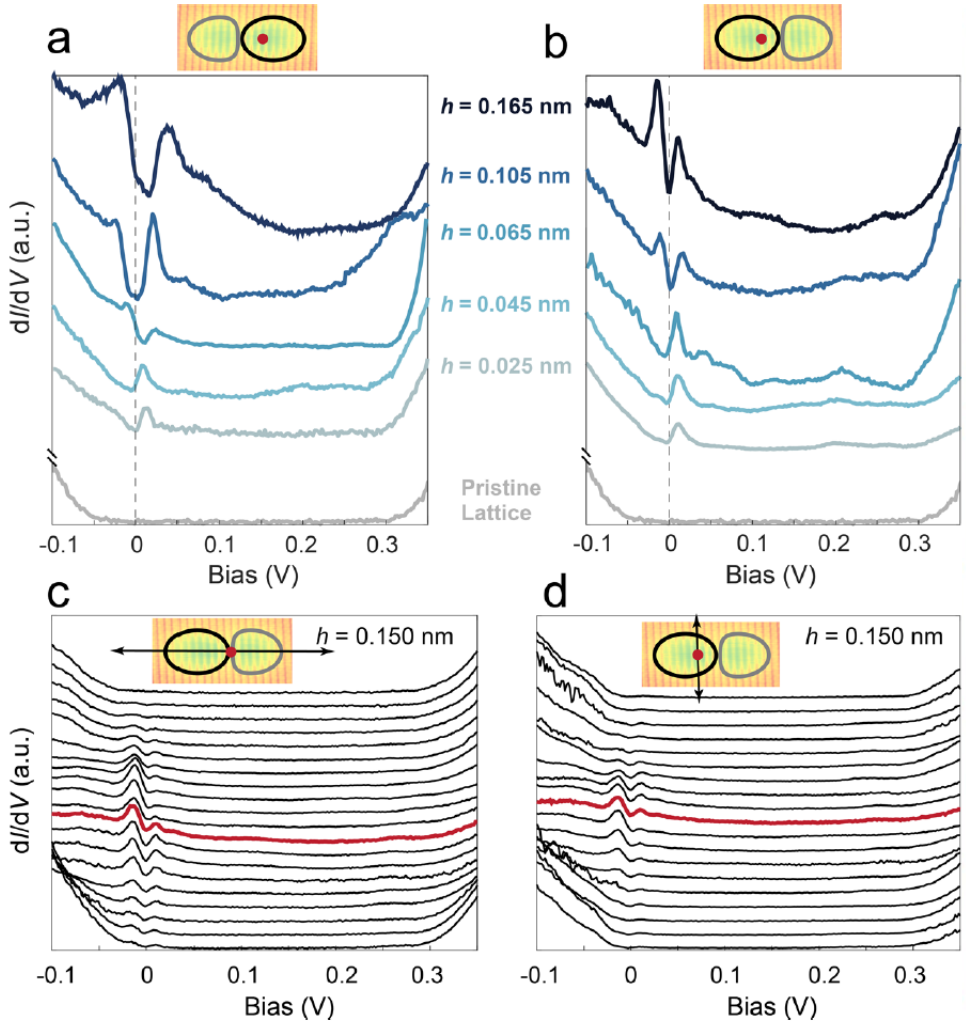

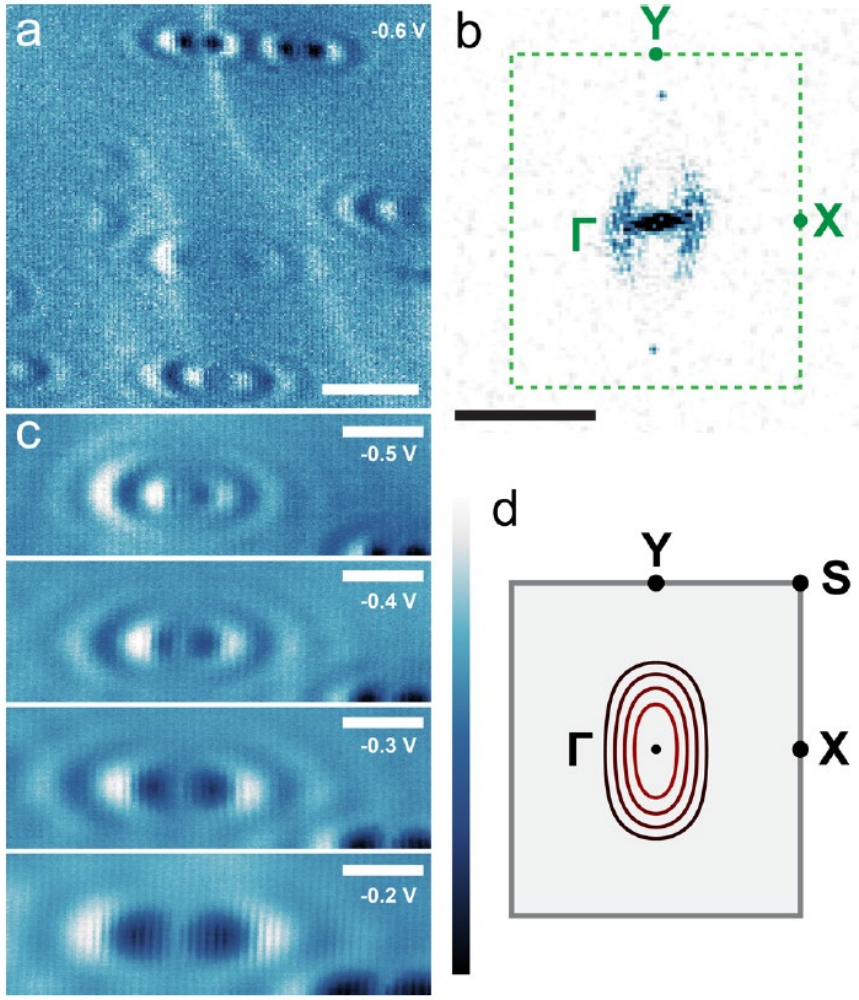

Friedel oscillations around vacancies

Vacancies in sublattice A and B, first and second layers

Co atom at black-P surface

ARTICLE

NATURE COMMUNICATIONS | (2018)9:3904

DOI: 10.1038/s41467-018-06337-4 OPEN

An orbitally derived single-atom magnetic memory

Brian Kiraly[1], Alexander N. Rudenko[1,2,3], Werner M.J. van Weerdenburg[1], Daniel Wegner[1], Mikhail I. Katsnelson[1] & Alexander A. Khajetoorians[1]

Several metastable configurations of Co atom, switching between them is possible betweet two states of hollow sites (top site is separated from them)

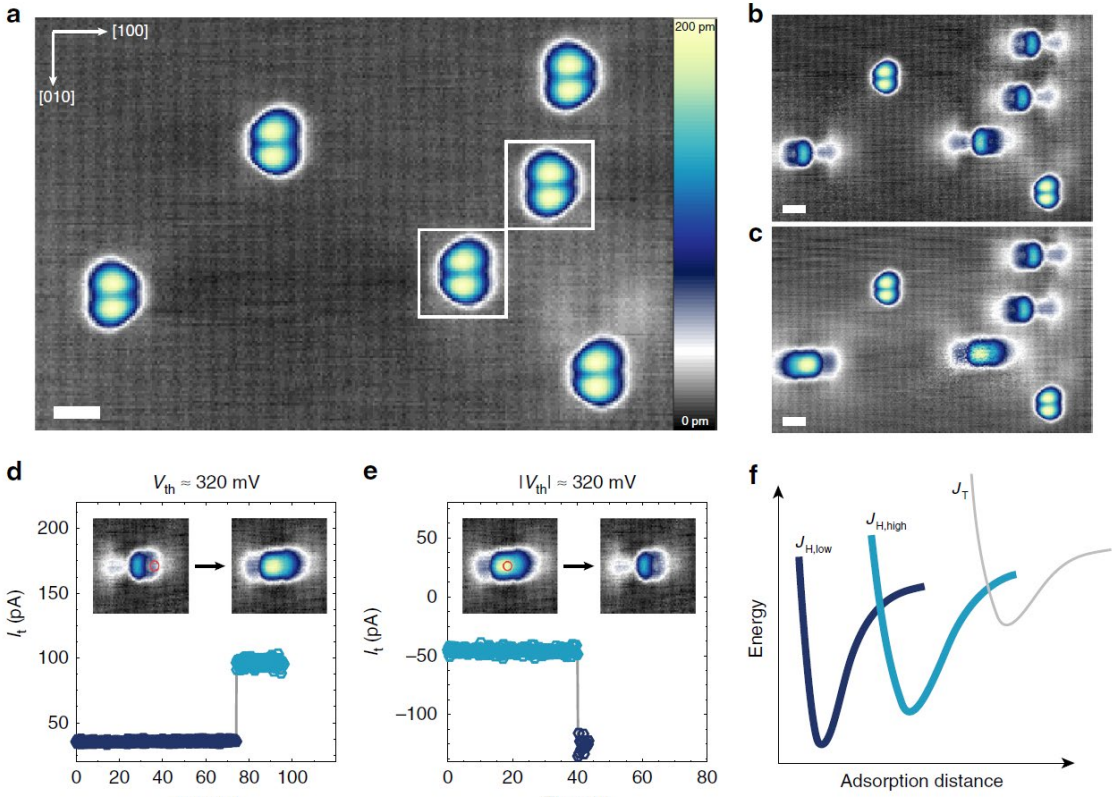

Fig. 1 Adsorption and switching of Co on BP. **a** Six Co species on BP as deposited at $T < 5$ K ($V_s = -400$ mV, $I_t = 20$ pA, scale bar = 1 nm). Boxed atoms show species related through mirror plane along [010]. **b** Four atoms from **a** have been switched into $J_{H,low}$ ($V_s = -400$ mV, $I_t = 20$ pA, scale bar = 1 nm). **c** Two atoms from **b** have been switched into $J_{H,high}$ ($V_s = -400$ mV, $I_t = 20$ pA, scale bar = 1 nm). **d** Switching characteristics from $J_{H,low}$ to $J_{H,high}$ with $V_s = 420$ mV and **e** $J_{H,high}$ to $J_{H,low}$ with $V_s = -680$ mV. Approximate threshold biases for switching (V_{th}) are noted. Orange circles indicate the tip position during the switching sequence. The inset images showing before and after configurations are 4 nm × 4 nm in size. **f** Schematic representation of adsorption energy curves for Co species on BP

Co atom at black-P surface II

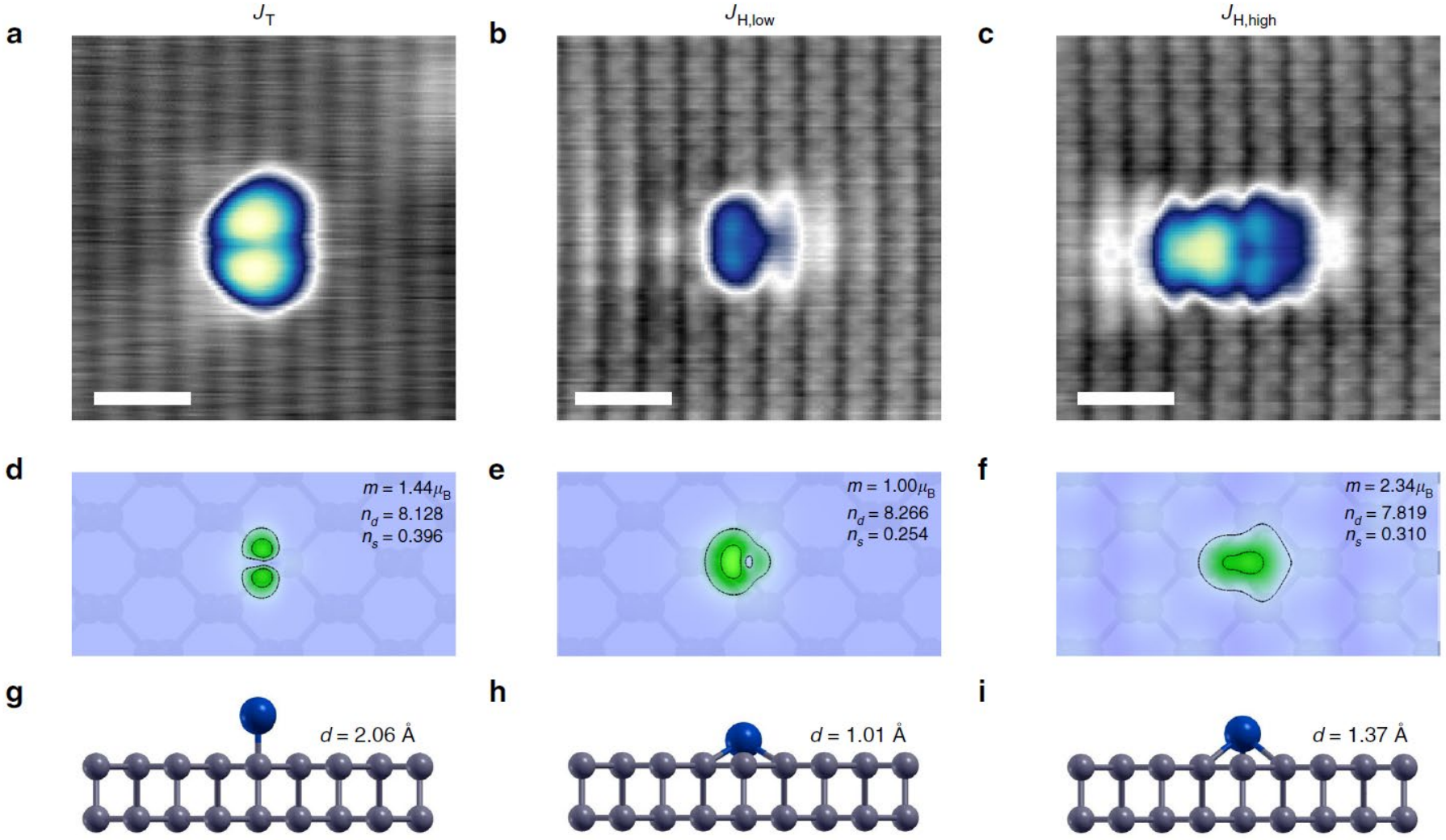

DFT+U calculations (U = 4 eV) confirm two metastable states for Co in hollow site

Co atom at black-P surface III

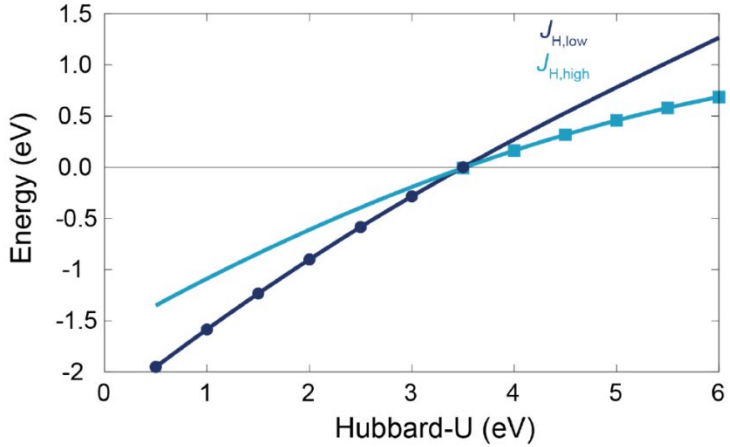

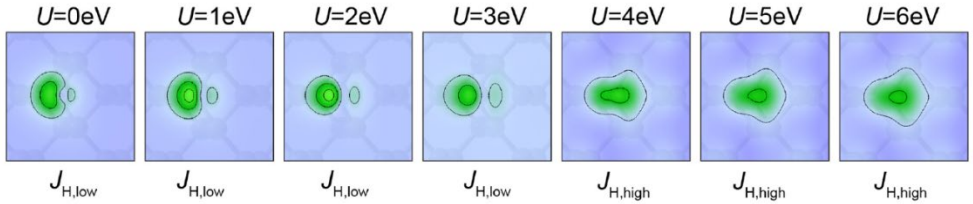

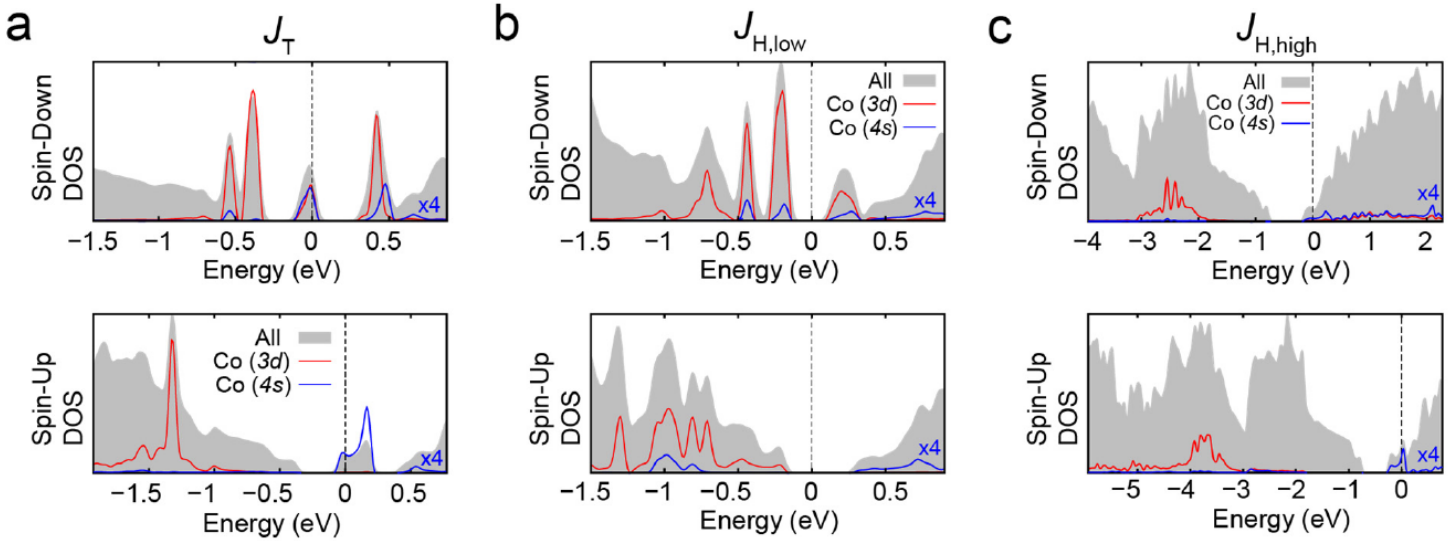

Exchange interaction of Co atoms

D. Badrtdinov, A. Rudenko, MIK, V. Mazurenko (2020)

$$\hat{\mathcal{H}}_{12} = J_{12}\hat{\mathbf{S}}_1\hat{\mathbf{S}}_2$$

Change of effective exchange interaction via orbital states of Co atoms

Different signs of interactions for high spin and low-spin configurations

Configuration	HH	HL	LL
Exchange interaction (meV)	13.3	4.8	-51.2
Co-Co distance R (Å)	4.34	4.47	4.37
Co-BP distance d (Å)	1.37	1.34/1.00	1.01
Total magnetic moment (μ_B)	4.20	3.00	2.00
Adatoms moments (μ_B)	1.91	1.91/0.55	0.81

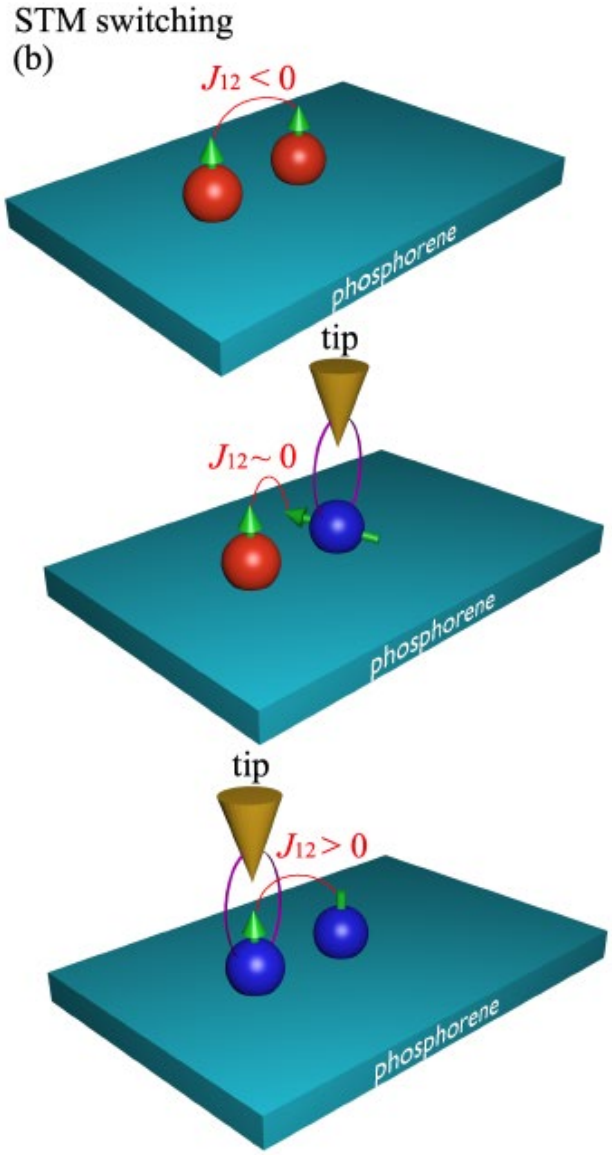

Exchange interaction of Co atoms II

Distance dependence of *J*

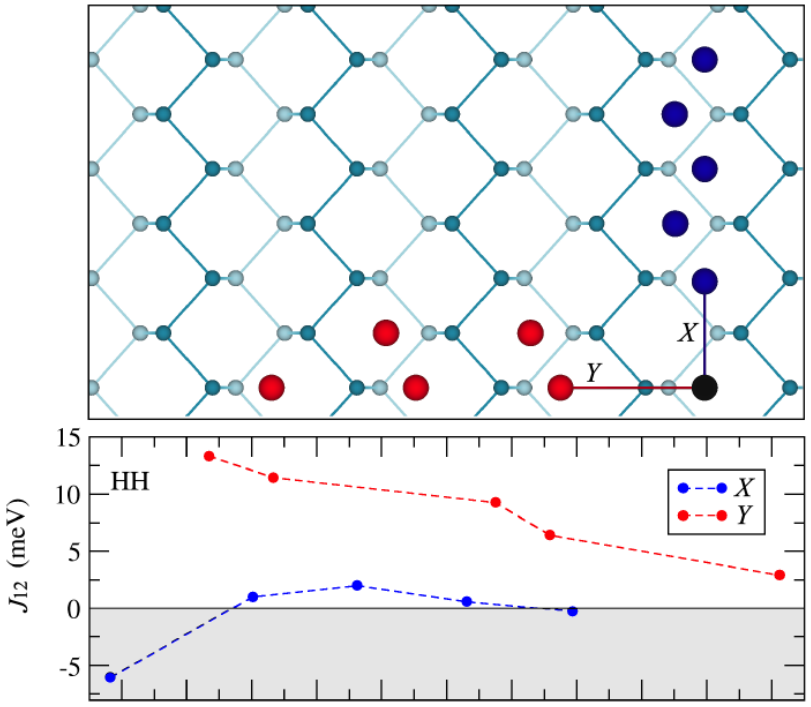

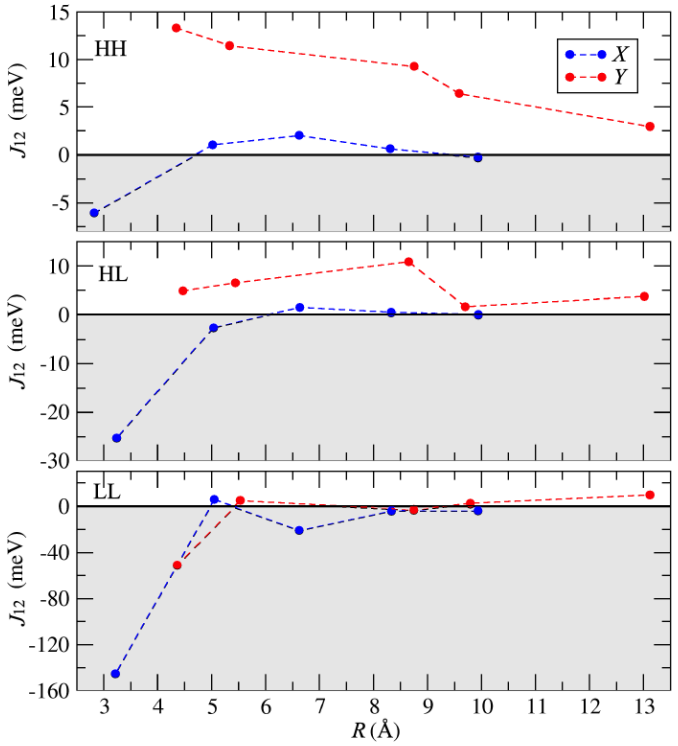

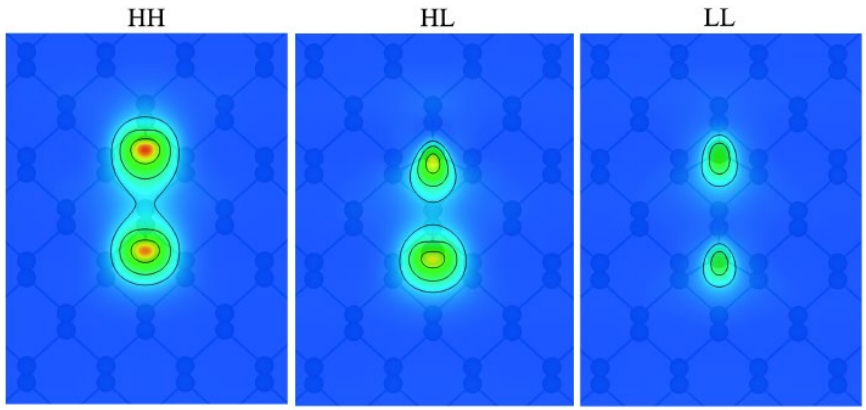

Charge density distributions
(H – high spin, L – low spin)

Exchange interaction of Co atoms III

Model analysis in two-site Anderson model

$$\hat{\mathcal{H}} = \hat{\mathcal{H}}_p + \hat{\mathcal{H}}_d + \hat{\mathcal{H}}_{pd},$$

$$\hat{\mathcal{H}}_p = \sum_{\sigma, i \neq j} t_{ij}^{||} \hat{c}_i^{\sigma\dagger} \hat{c}_j^{\sigma} + \varepsilon_0 \sum_{\sigma, i} \hat{c}_i^{\sigma\dagger} \hat{c}_i^{\sigma},$$

$$\hat{\mathcal{H}}_{pd} = V \sum_{\sigma} \sum_{i,j} (\hat{d}_1^{\sigma\dagger} \hat{c}_i^{\sigma} + \hat{c}_i^{\sigma\dagger} \hat{d}_1^{\sigma} + \hat{d}_2^{\sigma\dagger} \hat{c}_j^{\sigma} + \hat{c}_j^{\sigma\dagger} \hat{d}_2^{\sigma})$$

Magnetic force theorem

Δ **spin splitting**

$$J_{12} = \frac{1}{2\pi S^2} \int_{-\infty}^{E_F} d\epsilon \Im(\Delta G_{12}^{\downarrow}(\epsilon) \Delta G_{21}^{\uparrow}(\epsilon))$$

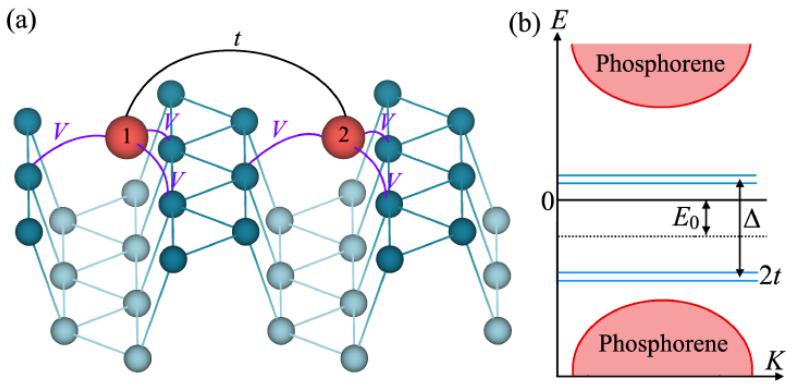

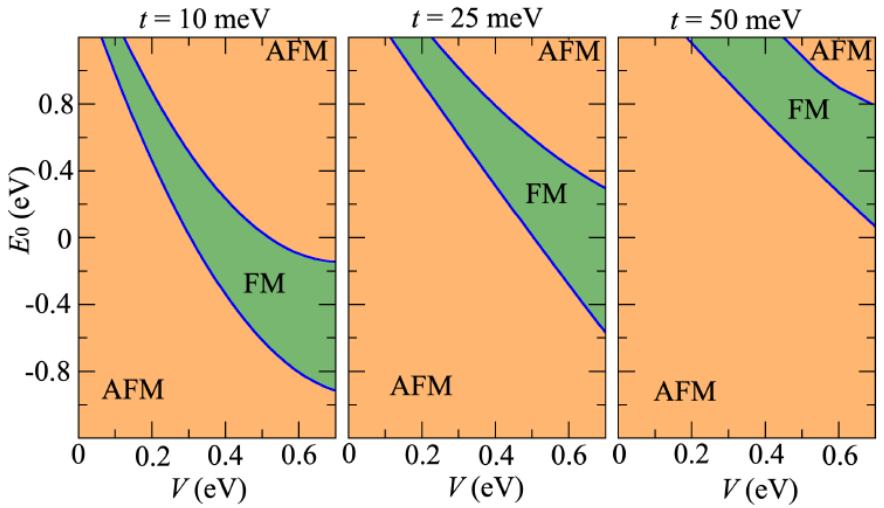

$\Delta = 1$ eV in all calculations

Screening and plasmons

D.A. Prishchenko, V.G. Mazurenko, MIK, and A.N. Rudenko, 2D Mater. 4, 027064 (2017)

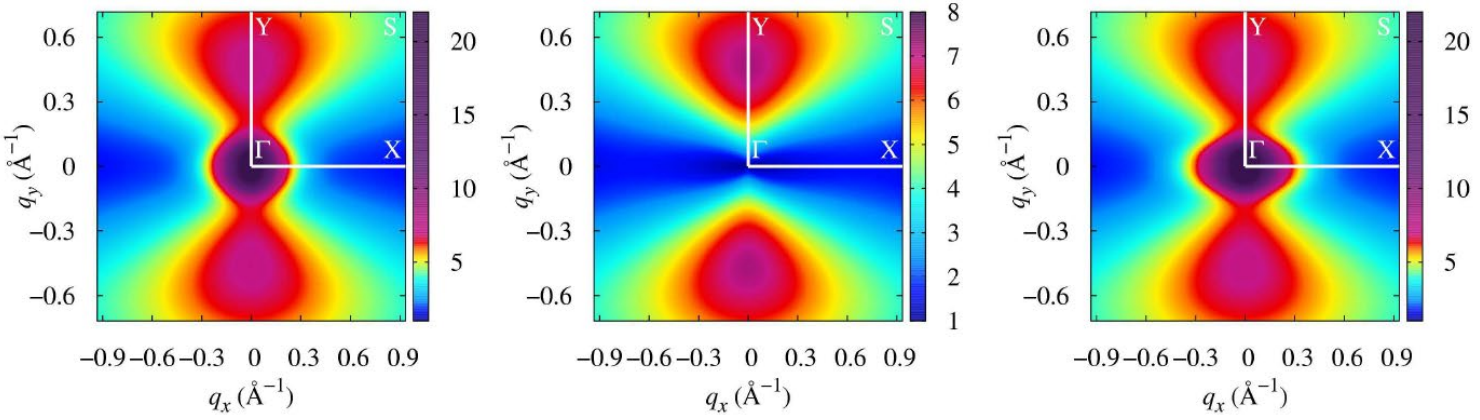

FIG. 4. Macroscopic static dielectric function $\epsilon_M(q_x, q_y)$ calculated for electron-doped (left), undoped (middle) and hole-doped (right) 1L-BP. Each plot shows distribution of ϵ_M over the whole BZ. Doping in both electron- and hole-doped cases corresponds to $n = 10^{13}$ cm^{-2}.

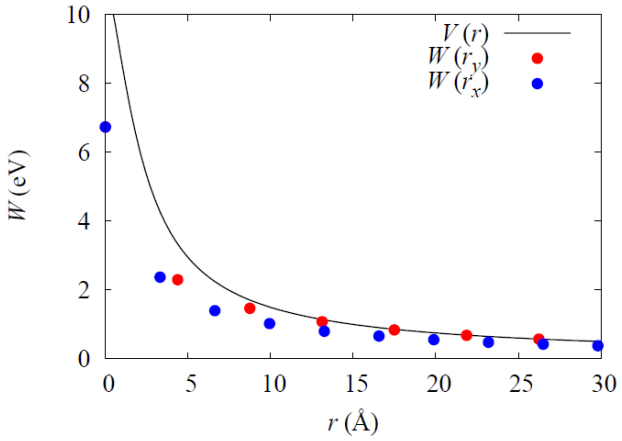

FIG. 5. Diagonal element of the screened Coulomb interaction matrix W calculated in real space along $x-$ (blue) and $y-$ (red) directions of 1L-BP. Unscreened (bare) interaction $V(r)$ is shown for comparison.

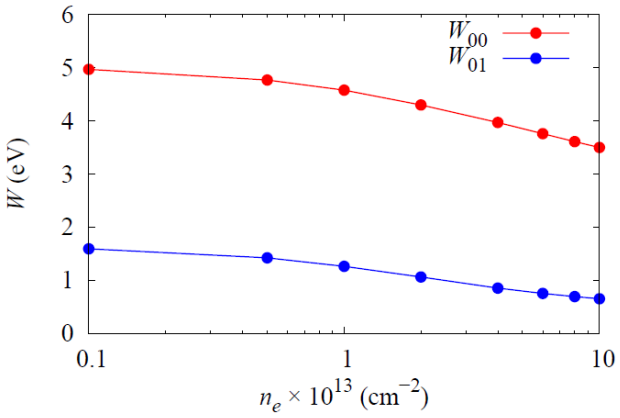

FIG. 6. On-site (W_{00}) and nearest-neighbor (W_{01}) screened Coulomb interaction in 1L-BP shown as a function of electron doping n_e. Red and blue lines are guide for the eye.

Screening and plasmons II

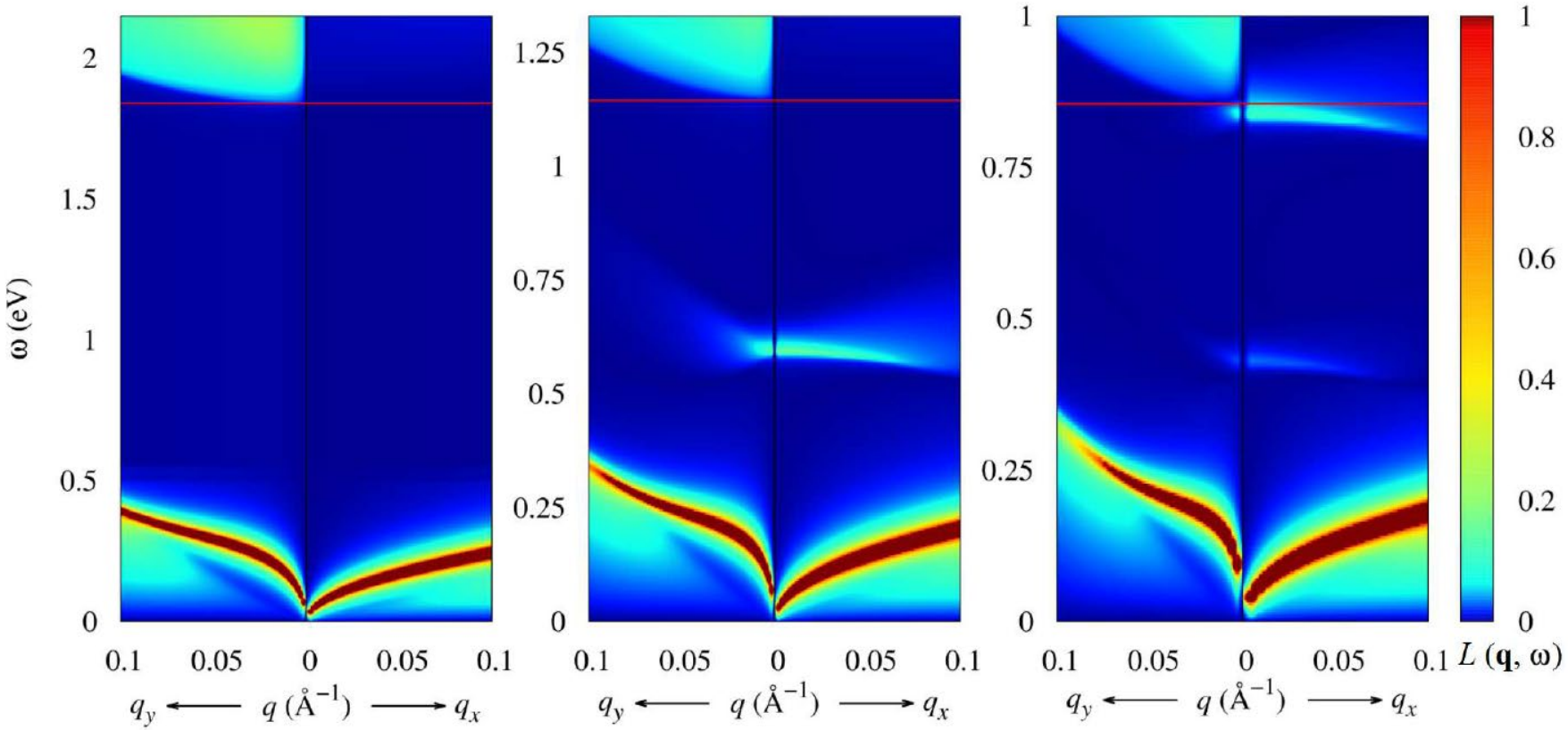

FIG. 7. Wave vector and frequency resolved loss function $L(\mathbf{q},\omega)$ (shown in color) calculated for 1L-, 2L-, and 3L-BP. Left and right part of each spectrum corresponds to $y-$ and $x-$ direction, respectively. Red horizontal line marks an energy gap for each system. Note different scales along vertical (ω) axis. In all cases, electron-doping was used, corresponding to $n_e = 10^{13}$ cm^{-2}.

Screening and plasmons III

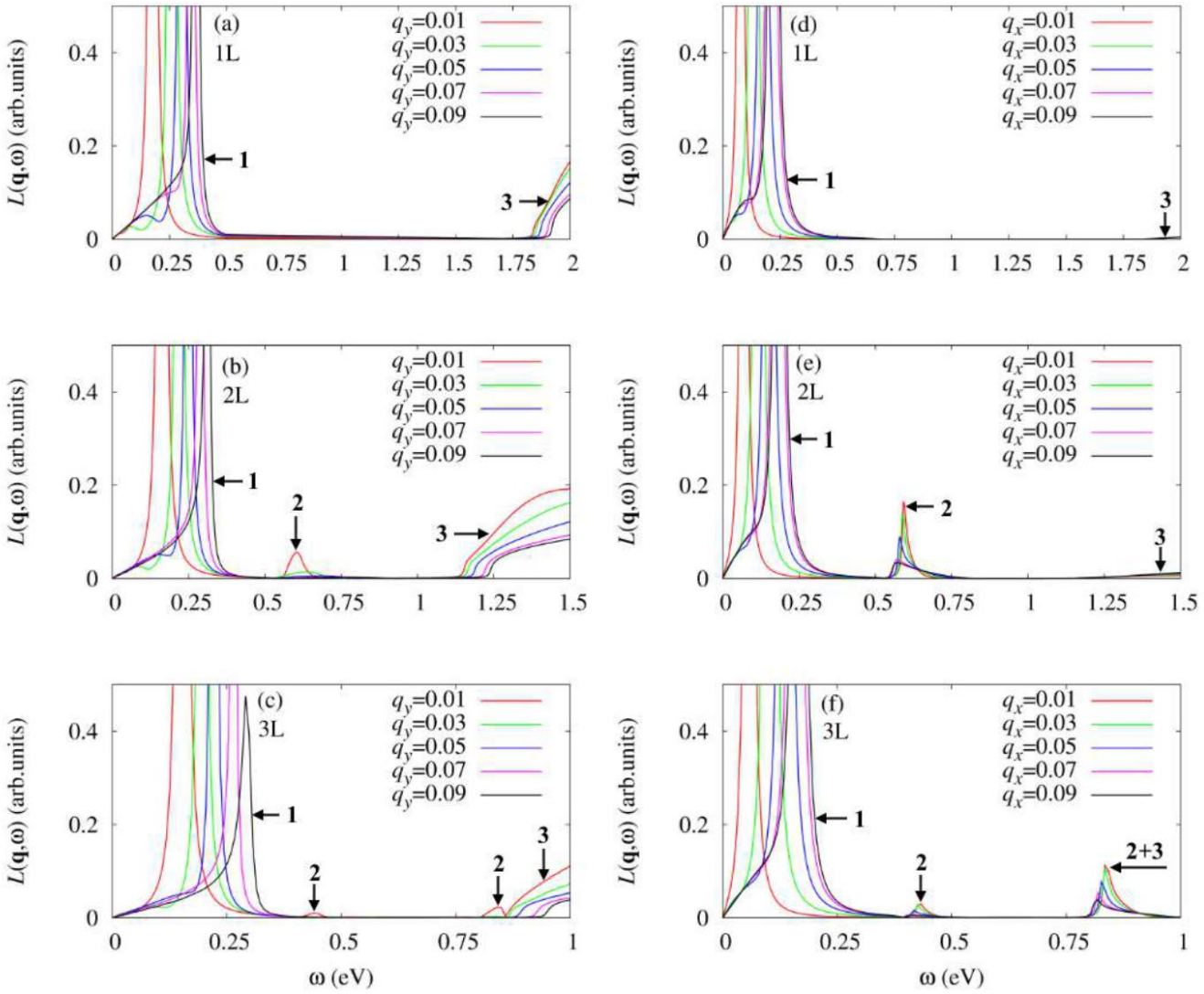

EELS function for 1, 2, 3 layers of phosphorus: several plasmon branches are seen

Anisotropic screening: experiment

Alex Khajetoorians group (Nijmegen)

B. Kiraly et al, PRL 123, 215403 (2019)

Ordering of K at black P surface

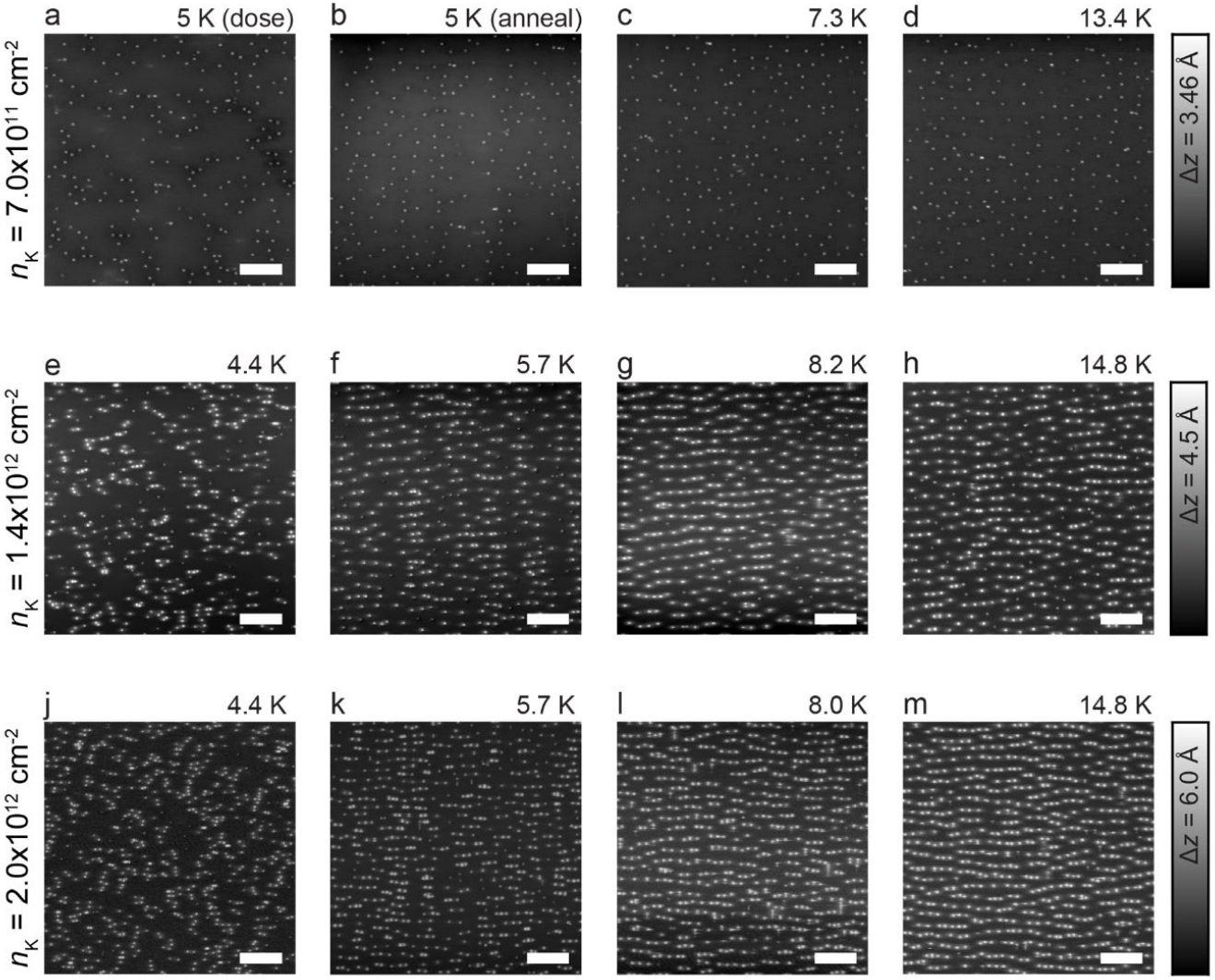

Anisotropic screening: experiment II

Potassium atoms form chains in the directions where screening is the strongest

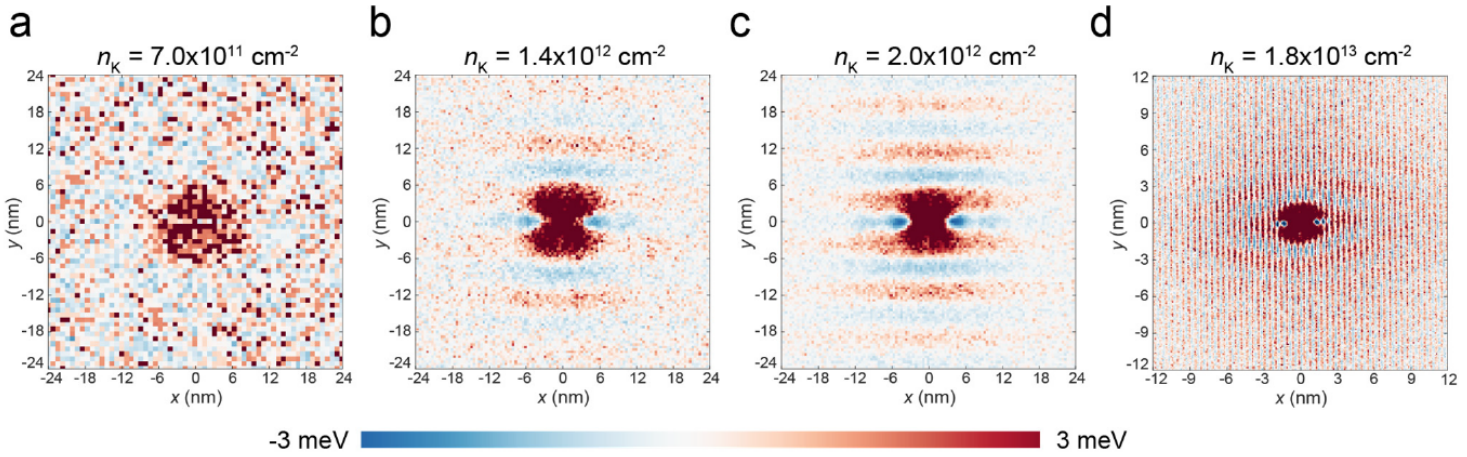

Figure 3. Density-dependent mean interaction potentials. Mean interaction potentials for varying K adatom density (n_K) are shown after annealing the samples to 13.4 K (lowest density), 14.8 K (medium and high density), and approximately 18.0 K (highest density). (a) Mean interaction potential for lowest K density (n_K = 7.0x10^{11} cm^{-2}) showing isotropic screening behavior. (b) Mean interaction potential at n_K = 1.4x10^{12} cm^{-2}, revealing the onset of screening anisotropy. (c), (d) Mean interaction potential for n_K = 2.0x10^{12} cm^{-2} and n_K = 1.8x10^{13} cm^{-2}, respectively.

Anisotropic screening: experiment III

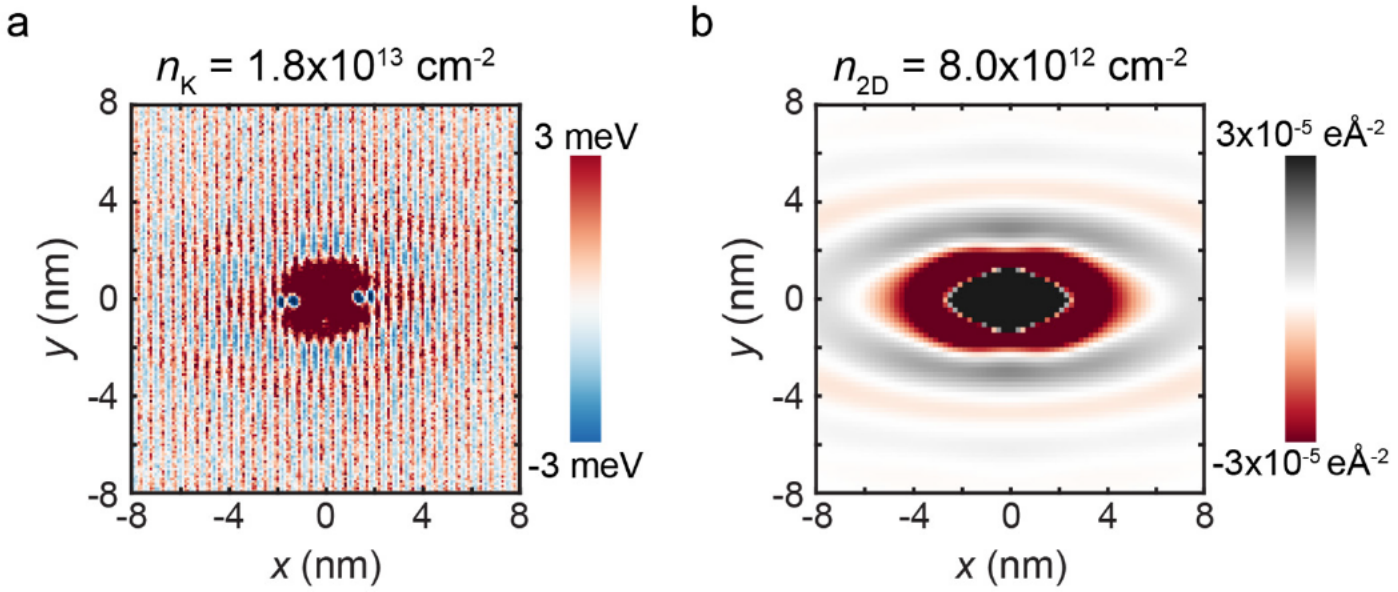

Supplementary Figure 8. Comparison between theoretical and experimental Friedel oscillations. (a) Mean interaction potential with n_K = 1.8x10^{13} cm^{-2} showing elliptical oscillatory envelope characteristic of free-carrier scattering on the Fermi surface. (b) Numerical calculation for charge-density redistribution around a single point charge on monolayer BP with E_F located 0.05 eV above the CB minimum (corresponding carrier density n_{2D} = 8.0x10^{12} cm^{-2}).

Anisotropic screening in agreement with theoretical predictions

Intrinsic mobility in single-layer BP

In graphene, two-phonon processes involving flexural phonons are more important that single-phonon processes involving in-plane phonons (except very low temperatures)

PRL 105, 266601 (2010) PHYSICAL REVIEW LETTERS week ending 31 DECEMBER 2010

Limits on Charge Carrier Mobility in Suspended Graphene due to Flexural Phonons

Eduardo V. Castro,[1] H. Ochoa,[1] M. I. Katsnelson,[2] R. V. Gorbachev,[3] D. C. Elias,[3] K. S. Novoselov,[3] A. K. Geim,[3] and F. Guinea[1]

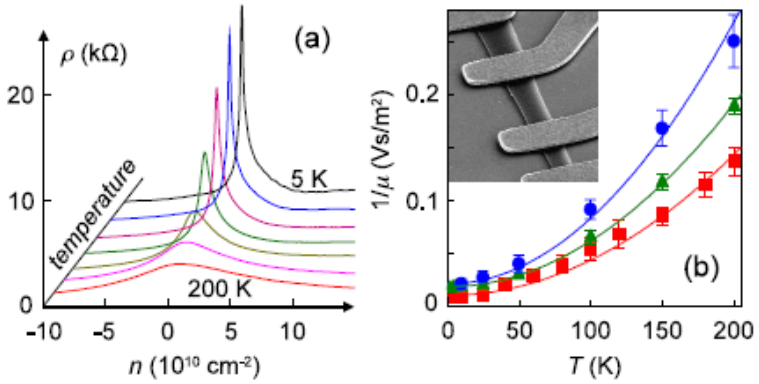

FIG. 3 (color online). (a) Electron transport in suspended graphene. Graphene resistivity $\varrho = R(w/l)$ as a function of gate-induced concentration n for $T = 5$, 10, 25, 50, 100, 150, and 200 K. (b) Examples of $\mu(T)$. The T range was limited by broadening of the peak beyond the accessible range of n. The inset shows a scanning electron micrograph of one of our suspended device. The darker nearly vertical stripe is graphene suspended below Au contacts. The scale is given by graphene width of about 1 μm for this particular device.

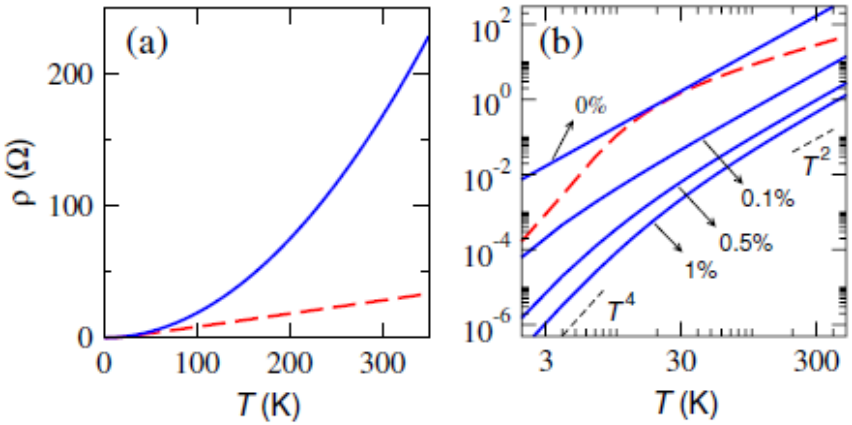

FIG. 2 (color online). (a) Contribution to the resistivity from flexural phonons (blue full line) and from in-plane phonons (red dashed line). (b) Resistivity for different strain. The in-plane contribution (broken red line) shows a crossover from a low to a high—T regime. In both cases, the electronic concentration is $n = 10^{12}$ cm^{-2}.

Intrinsic mobility in single-layer BP II

A. N. Rudensko, S. Brener, MIK, PRL 116, 246401 (2016) **What about black P?**

Kubo-Nakano-Mori formula (corresponds to variational solution of Boltzmann equation)
Phonon energies at $q = 2k_F$ are supposed to be much smaller than k_BT

$$\sigma_{xx} = \frac{e^2}{2S}\sum_{\mathbf{k}} \tau_{xx} v_{\mathbf{k}}^{x2}\left(-\frac{\partial f}{\partial \varepsilon_{\mathbf{k}}}\right) \qquad \frac{1}{\tau_{xx}} = \frac{1}{\langle j_x^2\rangle_e}\int_0^\infty \mathrm{d}t \langle F_x(t) F_x^\dagger\rangle$$

$$F_x = [j_x, H'] \qquad H' = \sum_{\mathbf{k}\mathbf{k}'} V_{\mathbf{k}\mathbf{k}'}^{\mathrm{eff}} c_{\mathbf{k}}^\dagger c_{\mathbf{k}'}$$

$$F_x = e\sum_{\mathbf{k}\mathbf{k}'} (v_{\mathbf{k}}^x - v_{\mathbf{k}'}^x) V_{\mathbf{k}\mathbf{k}'}^{\mathrm{eff}} c_{\mathbf{k}}^\dagger c_{\mathbf{k}'}$$

$$\mathbf{k} = \mathbf{k}' + \mathbf{q}$$

$$\frac{1}{\tau_{xx}} = \frac{\pi}{\hbar}\frac{\sum_{\mathbf{k}\mathbf{k}'} \delta(\varepsilon_{\mathbf{k}} - \varepsilon_{\mathbf{k}'})\left(-\frac{\partial f}{\partial \varepsilon_{\mathbf{k}}}\right)(v_{\mathbf{k}}^x - v_{\mathbf{k}'}^x)^2 \langle |V_{\mathbf{k}\mathbf{k}'}^{\mathrm{eff}}|^2\rangle}{\sum_{\mathbf{k}} v_{\mathbf{k}}^{x2}\left(-\frac{\partial f}{\partial \varepsilon_{\mathbf{k}}}\right)}$$

Parameters of interactions with in-plane and out-of-plane phonons are calculated from first principles

Continuum-medium derscription for in-plane and out-of-plane phonons

Intrinsic mobility in single-layer BP III

Energy dependence of effective masses are important (non-parabolic bands)

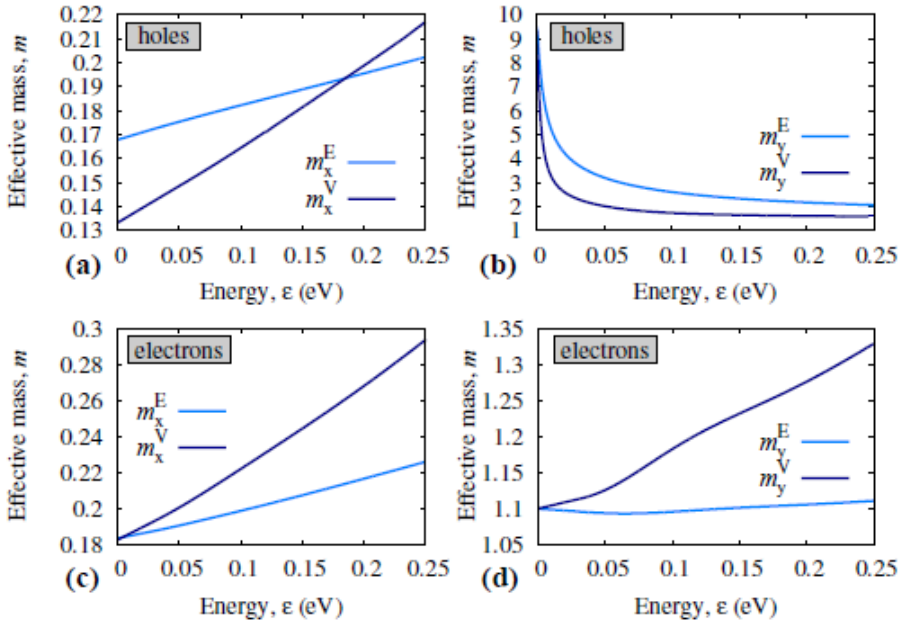

FIG. 5. (Color online) Energy dependence of the effective masses used in this work to approximate anisotropic dispersion (m_x^E, m_y^E) and band velocities (m_x^V, m_y^V) related to holes and electrons in monolayer BP.

$$\varepsilon_{\mathbf{k}} = \frac{\hbar^2 k_x^2}{2m_x^E(\varepsilon)} + \frac{\hbar^2 k_y^2}{2m_y^E(\varepsilon)} \qquad v_{\mathbf{k}}^{x(y)} = \frac{\hbar k_{x(y)}}{m_{x(y)}^V(\varepsilon)}$$

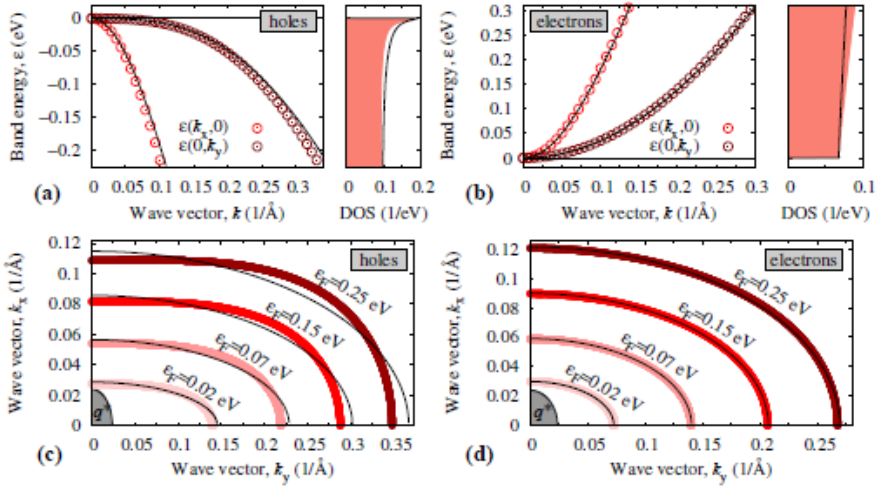

FIG. 2. (Color online) (a,b) Energy dispersion of electrons and holes in monolayer BP along the armchair (x) and zigzag (y) directions with the related densities of states (DOS). (c,d) Fermi contours $\varepsilon_F = \varepsilon(k_x, k_y)$ shown for the irreducible wedge of the Brillouin zone. Points and thick lines are the result of GW_0 calculations [32], whereas thin black lines correspond to the model used in this work. Gray area marks the phonon cutoff wave vector q^* at $T = 300$K (see text for details).

Intrinsic mobility in single-layer BP IV

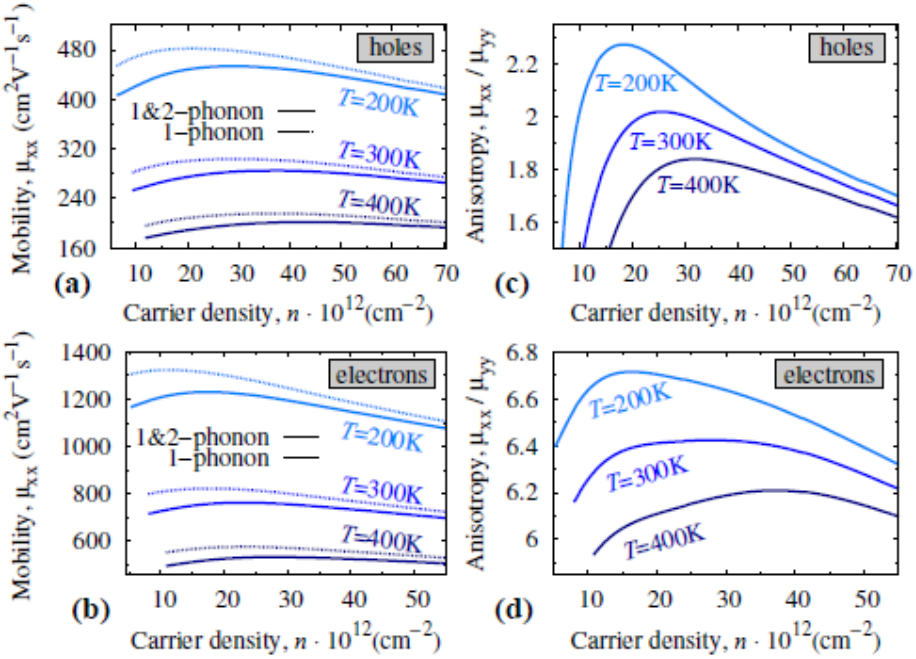

FIG. 3. (Color online) (a,b) Intrinsic carrier mobility (μ_{xx}) of monolayer BP shown as a function of the carrier concentration (n) calculated along the armchair direction for different temperatures (T). (c,d) Anisotropy of the carrier mobility represented at a ratio between the mobilities along the armchair and zigzag direction (μ_{xx}/μ_{yy}) shown for different T. Solid lines correspond to the contribution of both single-phonon and two-phonon scattering processes, whereas dashes lines to the single-phonon processes only. The lowest depicted density corresponds to the regime with $\ln(\bar{k}/q^*) > 1$.

Conclusions:

(1) Contrary to graphene, single-phonon processes are more important @RT;

(2) Intrinsic limit of mobility @R250 (700) $\mathrm{cm^2V^{-1}s^{-1}}$ for holes (electrons)

contrary to 10,000 for graphene;

(3) Anisotropy of mobility is much strongre for holes than for electrons

(2),(3) seem to be in qualitative agreement with experiments on a few-layer phosphorus

Flexuron tail of density of states

PHYSICAL REVIEW B **82**, 205433 (2010)

Flexuron: A self-trapped state of electron in crystalline membranes

M. I. Katsnelson

At finite temperature, membranes are rippled

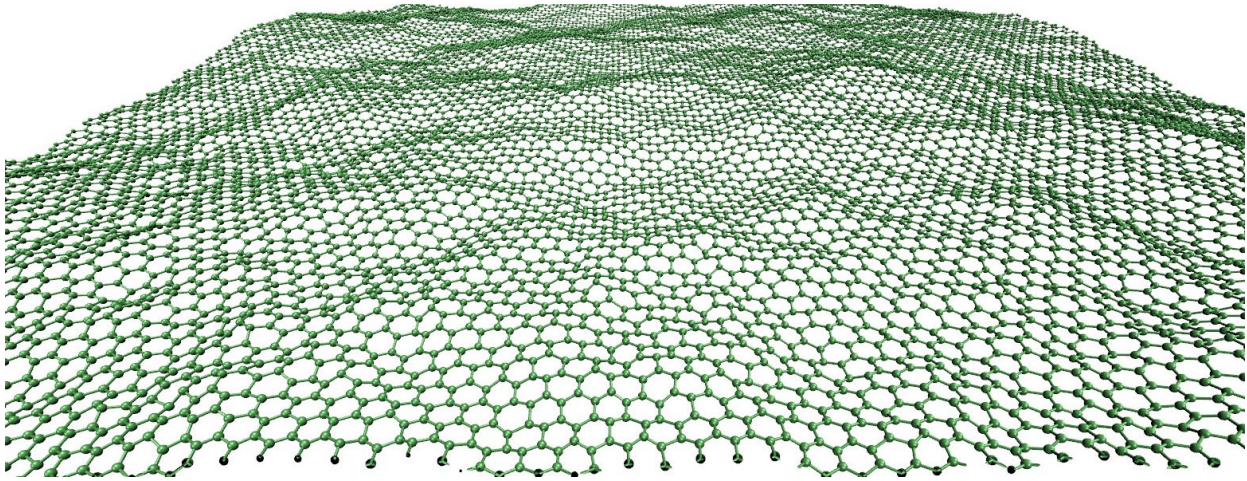

Snapshot: graphene @RT

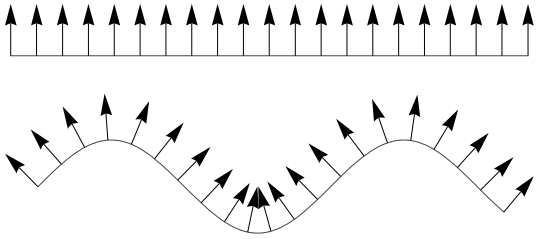

Interaction with intrinsic ripples – the same as two-phonon processes

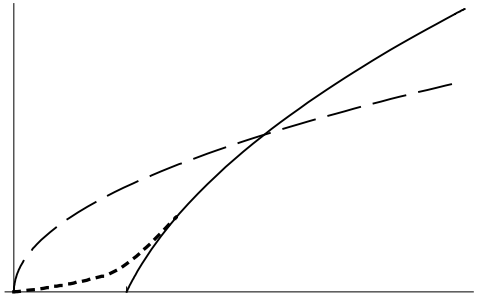

Average position of band edge is shifted and fluctuation tail appears (flexuron states)

Flexuron tail of density of states II

PHYSICAL REVIEW B **95**, 041406(R) (2017)

Effect of flexural phonons on the hole states in single-layer black phosphorus

S. Brener, A. N. Rudenko,* and M. I. Katsnelson

Electron self-energy $\Sigma(E,p) = \int \frac{d^2q}{(2\pi)^2}\gamma(p-q,p,q,E)K_2(q)G(E,p-q)$

Without vertex corrections: self-consistent Born approximation. To take into account fluctuation tail (idea of L.V. Keldysh)

$\gamma(p,p,0,E) = 1 - \frac{\partial\Sigma}{\partial E}$ Ward identity $\Sigma(E) = \left(1 - \frac{\partial\Sigma}{\partial E}\right)\int \frac{d^2q}{(2\pi)^2}\frac{K_2(q)}{E - \epsilon_q - \Sigma(E)}$

Applied to holes in phosphorene, parameters from ab initio calculations:

$\epsilon_q = 2.9q_x^2 + 0.05q_y^2 + 13.2q_y^4$ (atomic units)

Very anisotropic spectrum!

Flexuron tail of density of states III

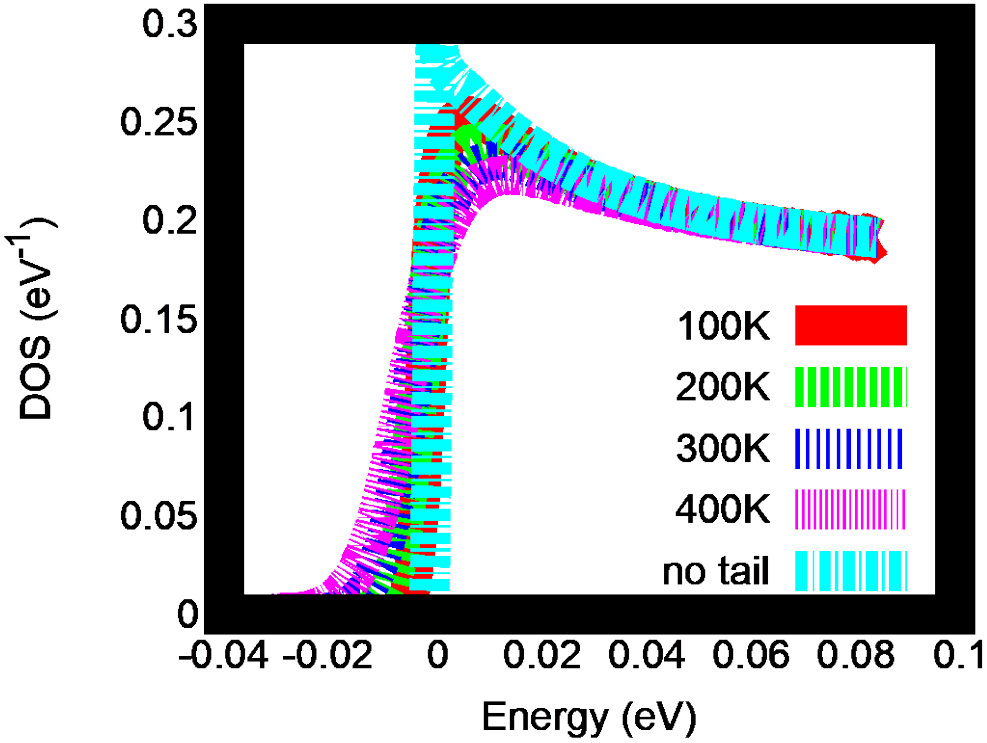

FIG. 1. DOS per unit cell per spin for T = 100, 200, 300 and 400 K. For reference, the DOS corresponding to bare dispersion without the inclusion of the flexuron tail is shown. The Van Hove singularity in the latter manifests the aforementioned quasi-one-dimensionality of the holes in black phosphorus. It is to a large extent smeared by the flexural modes.

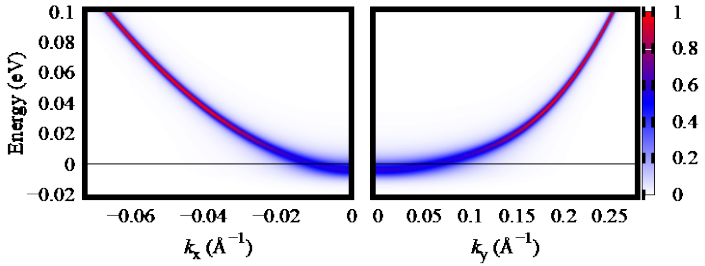

FIG. 2. Spectral function along k_x and k_y axis for T = 300 K. Note the different scale for the two plots.

Smearing of Van Hove singularity near the band edge by interaction with intrinsic ripples

Resume

(1) Completely different physics from both graphene and transition-metal dichalcogenides
(2) Strong difference of elecrtonic structure from monolayer to bulk despite small cohesive energy
(3) Insulator-semimetal transition under bias/potassium doping with anisotropic Dirac cones in bilayer black phosphorus
(4) Very interesting defects, especialy Co adatoms (single-atom orbital memory?!)
(5) Tunable electronic structure by hohg-frequemcy fileds?!
(6) Hyperbolic plasmons?!
(7) Mechanisms of intrinsic mobility quite different from graphene, much stronger interaction with acoustic phonons, strong limits on mobility

MANY THANKS
FOR YOUR ATTENTION